

LIBRARY Michigan State University

This is to certify that the

thesis entitled

AN EMBEDDED-TOW MODEL FOR CRUSH SIMULATION OF TEXTILE COMPOSITE TUBE

presented by

Chee-Kuang Kok

has been accepted towards fulfillment of the requirements for

MS ___degree in __Engineering Mechanics

Major professor

Date 8/10/01

MSU is an Affirmative Action/Equal Opportunity Institution

PLACE IN RETURN BOX to remove this checkout from your record. TO AVOID FINES return on or before date due. MAY BE RECALLED with earlier due date if requested.

DATE DUE	DATE DUE	DATE DUE
NOV 1 9 2002		

6/01 c:/CIRC/DateDue.p65-p.15

AN EMBEDDED-TOW MODEL FOR CRUSH SIMULATION OF TEXTILE COMPOSITE TUBE

Ву

CHEE-KUANG KOK

AN ABSTRACT OF A THESIS

Submitted to
Michigan State University
in partial fulfillment of the requirements
for the degree of

MASTER OF SCIENCE

Engineering Mechanics in Mechanical Engineering

2001

Professor Ronald C. Averill

ABSTRACT

AN EMBEDDED-TOW MODEL FOR CRUSH SIMULATION OF TEXTILE COMPOSITE TUBE

By

Chee-Kuang Kok

An embedded-tow model was developed to simulate the response of a circular triaxially-braided textile composite crush tube. The embedded-tow model was conceived from preliminary simulations of crush tube response using its parent model, the simplified discrete-tow model. Unlike the discrete-tow model, which represents the fiber tows and resin as beam and shell finite elements respectively, the embedded-tow model incorporates the fiber tows and resin into shell finite elements. Progressive failure of individual tow and resin is accounted for separately. The composite micro-constituent contribution to the overall composite macro-mechanical properties is represented using the micromechanical approach similar to the one adopted in the discrete-tow model. With a FORTRAN algorithm to model the composite non-linear material properties and the use of ABAQUS/EXPLICIT software code for simulation in the present study, the embedded-tow model proves its ability to predict the crush tube behavior under compression with adequate computational efficiency. The potential of the model to predict general triaxially-braided composite structure response is yet to be studied.

Copyright by CHEE-KUANG KOK 2001 To my parents, sister and brother, and my church family

ACKNOWLEDGMENTS

This work was partially sponsored by the Department of Energy and the Automotive Composites Consortium under USAMP/DOE Co-operative agreement DE – FC05 – 95OR22363. I would like to express my gratitude for the financial support. I would also like to thank Dr. Averill for his timely advice, insightful knowledge and great patience that went into this work. I thank my former colleague, Craig Carrier, for helping me along in the early stages of this work. Last but not least, I owe this work to all who have given me tremendous moral support.

TABLE OF CONTENTS

LIST OF TABLES	vii
LIST OF FIGURES	viii
CHAPTER 1 INTRODUCTION	1
1.1 Introduction	1
1.2 Literature Review	3
1.3 The Present Study	13
CHAPTER 2 PRELIMINARY MODELS	14
2.1 Introduction	14
2.2 The Checkerboard Model	15
2.2.1 Description of the Model	15
2.2.2 Numerical Results Using The Checkerboard Model	
2.3 The Cross-box Model	
2.3.1 Description of the Model	18
2.3.2 Numerical Results Using The Cross-box Model	19
CHAPTER 3 THE EMBEDDED-TOW MODEL	24
3.1 Introduction	24
3.2 Description of the Embedded-tow Model	25
3.2.1 Estimating Strains of Individual Components	26
3.2.2 Progressive Failure Schemes of	
Individual Components	27
3.2.2.1 Progressive Failure Algorithm	
3.2.3 Description of the Analysis	29
CHAPTER 4 EMBEDDED-TOW MODEL VERIFICATION AND	
CRUSH TUBE SIMULATION NUMERICAL RESULTS	
4.1 Introduction	
4.2 Material Properties	
4.3 Verification of the Embedded-tow Model	
4.3.1 Simple Bending On A Strip	
4.3.2 Simple Tension and Compression On A Unit Cell	
4.4 Effect of Loading Rate and Mass-scaling	
4.5 Crush Tube Numerical Simulation Results	41
4.5.1 Crush Tube Load Versus Displacement Curve and	
Damage Mechanism	
4.5.2 Parametric Studies	
4.5.2.1 Effects of Chamfer Modeling	
4.5.2.2 Effects of Friction	44

CHAPTER 5 CONCLUSION	54
5.1 Conclusions	54
5.2 Future Work	54
BIBLIOGRAPHY	56

LIST OF TABLES

	Computed macro-mechanical properties of the 0°/+45°/-45° triaxially-braided composite material of the 80k/12k crush tube	46
Table 4.2	Mechanical properties of the composite constituents	46

LIST OF FIGURES

Figure 2.1	A summary of the modeling procedure the isolation of a unit cell of a triaxially-braided composite material to the final discrete-tow model	20
Figure 2.2	Damaging scheme of individual shell and beam elements in the discrete-tow model	20
Figure 2.3	Crush tube model by the checkerboard model	21
Figure 2.4	Comparison between simulation results from checkerboard model to experimental results of load versus displacement of the crush tube	21
Figure 2.5	Crush tube modeled by the cross-box model. (a) A magnified view of the cross-box regions. (b) The whole crush tube, with cross-box region on the left	22
Figure 2.6	Comparison between simulation results from cross-box model to experimental results of load versus displacement of the crush tube	23
Figure 3.1	 (a) Half of a repetitive volume element; (b) Axial tows, braider tows and resin represented as material stacks before the application of classical laminate theory; (c) The overall anisotropic material block, as in a unit cell 	31
Figure 3.2	(a) Unit cell before deformation; (b) Unit cell after deformation	31
Figure 3.3	A stress-strain curve representing progressive failure scheme of each individual constituent in a unit cell	32
Figure 3.4	A summary of the progressive failure algorithm	33
Figure 3.5	(a) Force applied at the platen, which moves towards the initiator, as in the experiment. (b) Initiator moves towards the tube in current simulation	34
Figure 4.1	A simple bending analysis on a strip of shell elements. Two bending forces, each of P/2 in magnitude, were applied into the plane	47

Figure 4.2 Comparison between the simulated and the theoretical out-of-plane displacements of the end of bending strip4	17
Figure 4.3 Comparison between the simulated and the theoretical bending stresses of the end of bending strip4	8
Figure 4.4 Uniaxial tensile and compressive test on a unit cell4	8
Figure 4.5 Stress-strain curve of a unit cell subjected to tensile force4	.9
Figure 4.6 Stress-strain curve of a unit cell subjected to compressive force4	.9
Figure 4.7 The effects of loading rate on the simulated strip out-of-plane displacement5	0
Figure 4.8 The effects of different mass scaling on the simulated strip out-of-plane displacement5	0
Figure 4.9 Simulated and experimental load versus displacement curve5	51
Figure 4.10 Simulated and experimental load versus displacement curve	51
Figure 4.11 Modeling the chamfer. (a) The chamfer as in the tube specimen (b) Chamfer modeled with one shell element lengthwise (c) Chamfer modeled with three shell elements lengthwise	52
Figure 4.12 Effects of chamfer modeling on the load versus displacement curve	52
Figure 4.13 Effects of Coulomb friction on the load versus	5.3

Chapter 1

INTRODUCTION

1.1 INTRODUCTION

Composite laminates have been used in the aerospace industry for many years, and efforts have been made to introduce their use in the automotive industry. Traditional composite laminates are known for their high in-plane stiffness and low weight. However, they do not consider out-of-plane stiffness and strength. To achieve better out-of-plane mechanical properties, woven textile composites were introduced as an alternative to traditional composites. With fiber bundles woven to form a cloth preform before resin impregnation, textile composites not only possess high in-plane stiffness and strength, but also helps improve out-of-plane strength. They are less likely to delaminate and thus are capable of carrying transverse loads.

However, unlike the traditional composite laminates, which can be analyzed by classical laminate theory, reliable yet computationally efficient formulations to relate the mechanical properties of textile composites have not been finalized. These mechanical properties include elastic constants and strengths to their micro-mechanics properties such as fiber architecture, fiber volume fraction and laminate configurations. Over the years, researchers have tried different approaches to model the behavior of textile composites and have

conducted numerous experiments, ranging from simple tensile tests to crush composite tubes, whose application is of interest in the present work.

An automotive crush tube is a structure that is part of the front rail of a vehicle, which is designed to absorb crash energy during a collision and thus prevent car passengers from high impact injuries. Traditionally manufactured using metal, textile composites are now thought of as a potential alternative due to their high specific impact resistance and energy absorption.

The goal of the present research is to simulate, using a finite element analysis, the response of a triaxially-braided textile-composite-based automotive crush tube subjected to axial compression. First, a simple yet computationally efficient strength and stiffness prediction model named the simplified discrete tow model was selected to model the entire crush tube. This model identifies a repetitive unit in the triaxially-braided composite material known as a unit cell, and represents the fiber bundles and the resin in the unit cell as beam elements and shell elements respectively. A commercial finite element software, ABAQUS, was then employed to simulate the crush tube behavior, along with the use of a FORTRAN algorithm to model the material non-linearity.

A brief literature review concerning the various textile composite stiffness and strength models, together with related experiments performed on textile-composite crush tube are presented as follows.

1.2 LITERATURE REVIEW

The attractiveness of textile composites lies in their in-plane mechanical properties being comparable to their traditional laminates counterparts, their improved out-of-plane strength and impact resistance, their ability to conform to irregular shapes, and their relative manufacturability. Yet, all these desirable features come with a price. Due to their micro-structural complexity, textile composite materials are difficult to analyze, let alone textile composite structures.

Since the size of tow and unit cell are usually within the same order as the important geometrical features of textile composite base structures, the microstructures of textile composite are too complicated and computationally costly to be modeled explicitly, yet too distinct to be "smeared out" using a homogenization scheme. In fact, this is the primary difficulty in the design of an optimum textile composite architecture. However, researchers have sought after different approaches, varying in the degree of simplifications, to come up with approximate solutions to the problem at hand. Many solutions on how to predict textile composite stiffness have been presented, but not as many have been extended to predict the material strength. Efforts to incorporate these models into a textile composite structure to simulate the structural response are even scantier.

Most researchers have approached the problem of textile composite stiffness and strength modeling by first identifying a repetitive region in the textile composite, or a unit cell, that can be duplicated into an entire composite. This unit cell approach usually involves a type of volume averaging from the onset, and is based on strength of material theory, classical lamination theory or a homogenized finite element technique.

Early researchers Ishikawa and Chou [1,2,3] developed three models to model plain weave, twill weave, four harness satin and eight harness satin composites. Their mosaic model regarded the textile composite as an assemblage of cross-ply laminates. By assuming iso-strain and iso-stress conditions, upper bound and lower bounds of composite stiffness were obtained. One-dimensional approximations were applied to strips of warp and fill strands, thus neglecting tow undulation. In their second model, the modified fiber undulation model [3], efforts were made to include tow continuity and undulation by applying classical laminate theory to each infinitesimal piece of strand-wise strips, with further assumption of successive failure of strands transverse to applied load. The knee phenomenon that characterizes fabric behavior after initial strand failure was studied using this model. Ishikawa and Chou had, in fact, adopted a progressive failure strategy in this model. The strands transverse to loading were first failed at their highest strain region, found to be at the center of undulation. The failed region moduli were reduced significantly, allowing damage to propagate until the whole strand had failed. Ishikawa and Chou also

introduced a third model [3], namely a bridge model to analyze satin weaves. This model contained a weak interlaced region among four surrounding stronger bridge regions to transfer loads. Progressive failure was again adopted to study knee phenomenon in satin weave composite using the bridge model.

Yang et al. [4] presented a fiber inclination model based on a modified classical laminated plate theory that regarded the unit cell as an assemblage of four inclined unidirectional laminae of the same thickness and the same fiber volume fraction. The unit cell, constructed by fiber bundles oriented in the diagonal directions, assumed the shape of a parallelepiped with its size determined by the weaving and braiding parameters. Though this approach could be extended to predict strength, it has a major drawback of ignoring fiber yarns interaction at the interlocking position and bending.

Whitcomb [5] conducted a three dimensional finite element analysis of plain weave composites to study the effect of tow waviness on the elastic constants and internal strain distribution of the composite. 20-noded isoparametric hexahedrons were used to model the unit cell. It was found that increasing tow waviness ratio increases normal and shear strain concentration under uniaxial loading. He, Woo and Gundapaneni [6] also developed a new type of finite element called macro finite element to account for the microstructure in the textile composite, rather than using the traditional finite element. This quadrilateral macro element contains sub-elements for modeling the tow, and

adopts a single field displacement approximation. Two-dimensional analyses performed suggested that the macro elements were capable in predicting global response but not local stresses or strains within the element. Whitcomb and Woo [7] then used this macro-element, together with a global/local strategy to reduce computational effort of textile composite analysis. In this method, a relatively crude global mesh was used to obtain the overall response of the structure. Refined local meshes were then used in the regions of interest where rapid stress changes may occur. Solutions were found accurate at regions remote from global/local boundaries. Whitcomb and Woo [8] later developed a multi-field macro-element and used it to study the effect of in-plane tow shift in a laminate consisting of two layers. In their analysis, a reduced sub-structuring technique was employed to obtain the macro-element stiffness matrix, and an enhanced direct stiffness method was used to assist the numerical analysis. Whitcomb and Srirengan [9, 10] also studied the sensitivity of predicted progressive failure to the quadrature order (the number of Gauss points) of elements used, mesh refinement, waviness ratio and choice of material degradation scheme of a plain weave composite subjected uniaxial loading.

The work of Naik and his colleagues included modeling of plain weave and triaxially-braided composite lamina elastic constants and strength as well as a laminate properties and behavior. In their earlier researches, Naik and Ganesh [11] developed a slice array model and an element array model that discretized a unit cell into slices and further divided each slice into elements to predict the on-

axis elastic properties of plain-weave composites. These slices and elements were then reassembled by imposing iso-stress and iso-strain conditions. Later in a series of publications, Naik and Ganesh [12,13,14] explained their geometry modeling of a plain weave lamina and laminate, then proceeded to develop an analytical model to predict the stress-strain history up to ultimate failure of 2D orthogonal plain weave fabric laminates under on-axis uniaxial static tensile loading, considering all the intermediate stages of failure. The stress analysis was conducted using the method of cells. Naik and Ganesh divided a unit cell into slices and subcells. To account for the nonlinearities of the strand and the matrix due to strand undulations and material progressive failure, iterations were performed on a unit cell by considering their stiffness convergence on the subcell level. To predict failure and model strength, final subcell stresses and average slice strain were compared to the permissible stresses and strains, with the failed region stiffness reduced accordingly. Using the same approach but different boundary conditions on the unit cell, Naik and Ganesh [15, 16] presented a failure analysis on plain weave composites under in-plane shear loading.

Naik et al. [17] employed a different approach in analyzing triaxially-braided composites. Here, transversely isotropic yarns were discretized along their path and interstitial matrix was represented as isotropic material slices. The constituent material mechanical properties were transformed to their corresponding values in global coordinates. A volume averaging technique was adopted to predict the composite stiffness. Naik [18, 19] then investigated

strength and failure mechanisms on a two-dimensional triaxially-braided composite, incorporating the effect of non-linear shear response of the constituent materials. A yarn bending model and a crack yarn model were introduced to study the details of tow failure.

Other researchers such as Dasgupta et al. [20] employed a homogenization scheme based on a realistic three-dimensional numerical simulation of simple plain-weave unit cell using the finite element method to investigate the interactions between micro-damage mechanisms and the macroscopic behavior of the composite. Similar to many other investigations, volume averaging of stress and strain fields was used to predict the overall composite properties. Takano et al. [21] also adopted a homogenization scheme but unlike Dasgupta et al. [20], macro-micro coupling between microscopic mechanical properties and the macroscopic structure was solved using four levels of hierarchy. Sankar and Marrey [22] presented an approach called selective averaging method (SAM) similar to that of Naik and Ganesh [16] to predict the thermo-elastic constants of textile composite materials. The unit cell was divided into slices and into elements, with the elastic constants of elements being averaged selectively for iso-strain and iso-stress conditions. Again, the elastic constants on the micro-mechanics level were related to those on the macro-mechanics level by volume averaging of stiffness or compliance matrices. Pastore and Yasser [23] performed a modification of Fabric Geometry Model [23] that related fiber architecture and material properties of textile reinforced composites to global stiffness through micro-mechanics and stiffness averaging techniques.

The on-going battle in textile composite modeling seems to be the need for accuracy and the demand of computational efficiency. Glaessgen et al. [24] had gone so far as to discretize the detailed architecture of a plain-weave textile to allow internal details of unit cell to be examined. On the other hand, Dadkhah et al. [25] suggested that any model more complicated than the simple model they proposed, which was based on classical laminate theory, might not be justified due to the inevitable variations in the textile architecture. Dahkhah's modified laminate model seemed capable in predicting the compressive strength of a two-dimensional braided composite, as verified by the use of kink band model utilizing experimental information. In fact, West and Adams [26] found that the axial yarn crimping on a two-dimensional triaxially-braided composite could reduce its compressive strength by as much as 30%. Masters et al. [27] also suggested that minor changes in the braid geometry led to disproportionate strength variations, as their empirical data showed. Experiments performed by Masters and Ifju [28] demonstrated significant effect of textile architecture on mechanical properties of the composite.

All the effort presented thus far demonstrated the capability of predicting elastic moduli and strength of lamina and laminate. However, most of them are only suitable for a small-scale analysis, as the modeling of a composite structure

by discretely modeling the tow and resin will be extremely computationally costly. Recently, Carrier and Averill [29] developed a novel approach that discretely model the tow and resin using beam and shell elements in the unit cell while considering the tow undulation and essential geometrical features. While losing accuracy due to simplification, this computationally efficient approach seem promising in approximating the response of a crush tube, and will thus be adopted in the current analysis.

With regard to material progressive failure modeling, a few common approaches are found in the literature. Hamelin and Bigaud [30] developed a multi-scale energy approach that minimized the strain energy complementary energy to predict the failure behavior of textile composite of different textile architectures. In this approach, three levels of size hierarchy from micro to meso and then macro were utilized. The stresses/strains of one hierarchy was then related from one to the other through the localization matrices. A failure criterion was chosen and progressive failure performed by changing the constitutive matrix of the meso-element using the selective RC (row and column) method. Tan and Nuismer [31] also presented a theory for progressive matrix cracking in traditional composite laminates. The appealing feature of this model is that, unlike other theories that require some empirical data on the laminate, only the basic material properties of constituent materials are needed to model progressive matrix cracking. However, the theory has yet to be extended for textile composite application. Blacketter et al. [32] adopted an

empirical stiffness reduction scheme and applied it to each failed Gauss point of a FEM-discretized textile composite material element to simulate different types of failure. Iterations were then performed to recalculate the stiffness matrix due to occurrence of material failure.

Literature on elastic constants and strength modeling are abundant, and a good summary of some of the work mentioned can be found in Tan et al. [33]. However, not as much analytical work has been performed on modeling the response of the composite tube subjected to axial compression. Mamalis et al .[34] developed an energy model to quantify the energy absorption of crush tubes with different geometries. Based on their experimental observation of fracture mechanisms of a tube axially crushed against a platen, they attributed the absorbed energy to that dissipated during crack propagation, frond axial splitting, frond bending and friction between exposed surfaces. Castejon et al. [35] performed a finite element simulation using ABAQUS/Explicit and DYNA3D to predict the mechanical behavior, the mean crash load and specific crash energy of an absorber, which has a more complex geometry compared to a simple crush tube. The absorber is analyzed using a biphase material of E-glass fiber and polyester resin instead of a textile composite material. Three crushing modes, namely local buckling, lamina bending and transverse shearing were identified and simulated. Hamada and Nakatani [36] presented three different finite element models to simulate the response of a simple axially-loaded textile composite crush tubes after initial crack using plain strain elements to represent tube wall, fronds and debris wedge, and truss elements to represent the contact region between fronds and wedge. However, it was not clear as to which model compared best to reality.

Masters and Minguet [37] conducted experimental investigation on the elastic moduli and strength of two-dimensional triaxially-braided textile composites. The study included the effects of primary braid architecture, namely the braid angle, axial tow content and yarn size and secondary architecture, namely the yarn crimp angle and yarn spacing, on the mechanical performance of the composite. Chiu et al. [38] conducted tube-crushing experiments on six different non-hybrid and hybrid types of 2D triaxially braided composite tubes containing Kevlar and carbon fibers to study their crush failure modes and specific energy-absorbing capabilities under guasi-static axial compression. The influence of fiber type and the hybrid structure on the crush failure mode, the specific energy-absorption and the load/displacement response were examined. Mamalis et al. [34] and Hull [39] performed thorough investigations on the fracture mechanisms of an axially-loaded crush tube and related the mechanism with the load-displacement curve. While Mamalis et al. believed that friction was the most important parameter affecting the energy absorption of the crush tube, as affirmed by Hamada and Nakatani's [23] finite element analysis, Hull pointed out that the specific crushing stress was the most useful and distinctive parameter to relate the performance of different materials and component geometries. Their work revealed the inter-dependency of material, geometrical and testing parameters and their difficult-to-quantify complexity.

1.3 THE PRESENT STUDY

In the present study, a finite element model is developed to efficiently simulate a two-dimensional triaxially-braided composite crush tube response subjected to uniaxial compression. The embedded-tow model derived from the simplified discrete-tow model [29] is adopted for the prediction of the composite crush tube behavior. Failure of individual elements, namely tows and matrix, with incremental compressive load represents the overall progressive failure of the composite tube. The tows and matrix are not explicitly modeled, rather collectively represented in shell elements. The commercial finite element code, ABAQUS/Explicit, is used to simulate the crush tube load-displacement behavior. Some preliminary models have been investigated before the current model is developed, and they are presented in Chapter 2. The tube modeling procedures are discussed in Chapter 3, and verification of the current model is presented in Chapter 4. The final chapter, Chapter 5, concludes the research by summing up important observations and possible extension of the ideas developed in this investigation to related application. Future areas of study are also recommended.

Chapter 2

Preliminary Models

2.1 INTRODUCTION

The problem of simulating the textile composite crush tube behavior depends mostly on developing a proper model. Prior to the final model, two preliminary models were developed. These models, namely the checkerboard model and the cross-box model, are the major theme in this chapter.

The checkerboard board model and the cross-box model are both inspired from the simplified discrete-tow model developed by Carrier and Averill [29]. The discrete-tow model suggests the modeling of triaxially-braided composite material using shell elements for the matrix material and beam elements for the axial tows and braider tows. The main advantage of this model, as its name suggests, is the capability to capture the behavior of individual tow elements in the composite material, thus enabling simulation of tow scissoring and tow sliding.

In the discrete-tow model, the braider-tow beams are connected to the matrix shell at its diagonal ends. The axial tow, while being slightly shifted to one side of the unit cell, could be represented as two beam elements attached to edge of the shell. The modeling procedure, starting from the isolation of a unit

cell from a triaxially-braided composite material to the final discrete-tow model are briefly summarized in Figure 2.1.

Each constituent element in the discrete-tow model follows its own failure scheme. The damaging mechanism is such that the element behaves elastically up to a peak load after which the element stiffness is greatly reduced until it reaches a post-damage region, as can be seen in Figure 2.2. In the post-damaged region, the element stiffness is so low that the failed material can be considered incapable of transferring load. The peak point before damaging is determined using different failure criteria. The tows are assumed to follow the maximum strain failure criterion, whereas the matrix is assumed to obey the maximum stress failure criterion.

2.2 THE CHECKERBOARD MODEL

2.2.1 DESCRIPTION OF THE MODEL

The checkerboard model is employed to explicitly model the crush tube. The word explicit here means that the crush tube constituents, namely the tows and the matrix material, are accounted for in the model as closely as possible with regard to their physical arrangement and dimensions. However, the adoption of the discrete-tow model mandated the use of two separate axial tows in a unit cell, which is only an approximation of the physical reality. Nevertheless, this approximation is desirable in the view that the anticipated response of the

symmetric model, resulting from the simplification, to symmetric boundary conditions will also be symmetric. This is more likely to match the crush tube behavior subjected to a compressive force from a circular initiator, since the crush tube is composed of the same textile material throughout, and the circular initiator should impose nearly uniform loading on the end of the crushing region. Any discrepancy from this expectation can only be attributed to imperfect specimen, uncontrollable testing parameters, or stress waves in the tube due to dynamic effects. Figure 2.3 shows a crush tube modeled using the checkerboard model.

The checkerboard model is able to capture the scissoring of braider tows and the sliding of the braider tows within the unit cell, but not the sliding with tows of neighboring cells. In addition, the sliding of axial tow with the braider tow is not represented since the tows are pinned at the nodes of the shell elements.

The axial tows are modeled as I-beams whereas the braider tows are modeled as rectangular beams. The use of I-beams and rectangular beams is an attempt to closely model the physical reality. Since the crush tube to be simulated consists of two layers of textile fabric, the axial tows are laying mostly at the top and bottom edges, which can be approximated with I-beams with very thin, thus negligible web sections. Since the braider tows are spread out uniformly in the fabric, they can be approximated as rectangular beams. The areas of the beams should be the same as the total area of the tows, as

computed using the approach presented in the work of Carrier and Averill [29]. The dimensions of the beams are found by performing finite element bending simulation on a strip of discrete-tow elements complete with beams and shells, and then comparing them to the results obtained from a strip of homogenized shell elements.

It is important to note that beams representing different tows should not be joined at the same node, since the moment of beam elements of different tows do not interfere with that of the neighboring tows. Beams of the same tow, however, should be joined at the same node. In fact, each tow should have its own node sets, and at the locations where a tow meet with its neighbors, only the displacements of the tow are tied to those of the neighboring tow of the same locations. In short, beams representing different tows should be pinned, not rigidly joined.

2.2.2 NUMERICAL RESULTS USING THE CHECKERBOARD MODEL

Computer simulation using the ABAQUS/Implicit finite element code was performed on the crush tube using the checkerboard model. The force-displacement curve of the experimental curve is compared to that of the simulation in Figure 2.4. These experimental results were obtained from [40]. The analysis diverged after a certain point, notably at the moment when severe damage had occurred on some elements. Owing to the presence of braider tows on alternate shell elements, the locations of damaging elements did not exhibit

symmetry. This was mostly due to early failure of sites unsupported by braider beams and was not what is to be expected physically, as the real tube should deform more uniformly. The divergence of the analysis was believed to have been caused by huge energy release when the axial and braider beams fail, resulting in numerical problems. Due to these issues, this model was deemed unsuitable for modeling tube behavior.

2.3 THE CROSS-BOX MODEL

2.3.1 DESCRIPTION OF THE MODEL

Due to the unsymmetrical deformation and the divergence of the analysis of the checkerboard model, the cross-box model was developed. Again, this model adopts the unit cell modeling from the discrete-tow model, but this time the physical arrangement of tows in the real tube specimen is neglected. In fact, the whole tube is deemed to consist of unit cells with matrix, braider tows and axial tows. To account for the discrepancy with the physical reality, the original volume fraction of matrix, axial tows and braider tows are maintained throughout the tube. Though this is more of an implicit modeling of the microstructure, it is expected to yield symmetrical deformation behavior.

This model can be a more refined model compared to the checkerboard model, but the increase of elements in refinement may reduce the efficiency of computation. Since the crush tube may not need to be totally crushed, the

uncrushed region may for the current analysis be represented with elastic shell elements with homogenized properties as those obtained from the discrete-tow model analysis. Figure 2.5 shows a crush tube modeled using the cross-box model. The cross-box region is magnified to assist visualization of the small elements. In modeling the beams, the same geometrical argument with regard to bending stiffness as applied to the checkerboard model is applied to the present model.

2.3.2 NUMERICAL RESULTS USING THE CROSS-BOX MODEL

Computer simulation using the ABAQUS/Implicit code was performed on the tube of cross-box model. The force-displacement curve obtained in the experiment [40] is compared to that of the simulation in Figure 2.6. Again, the analysis diverged after a certain point, notably at the moment when severe damage had occurred. Numerical problems were again suspected to be caused by high-energy release of the failing elements.

It is noted that the cross-box model actually over-predicts the stiffness of the composite crush tube. This discrepancy is not exhibited in the checkerboard model. It was suspected that the overall bending behavior of the tube might not be represented well using the cross-box model.

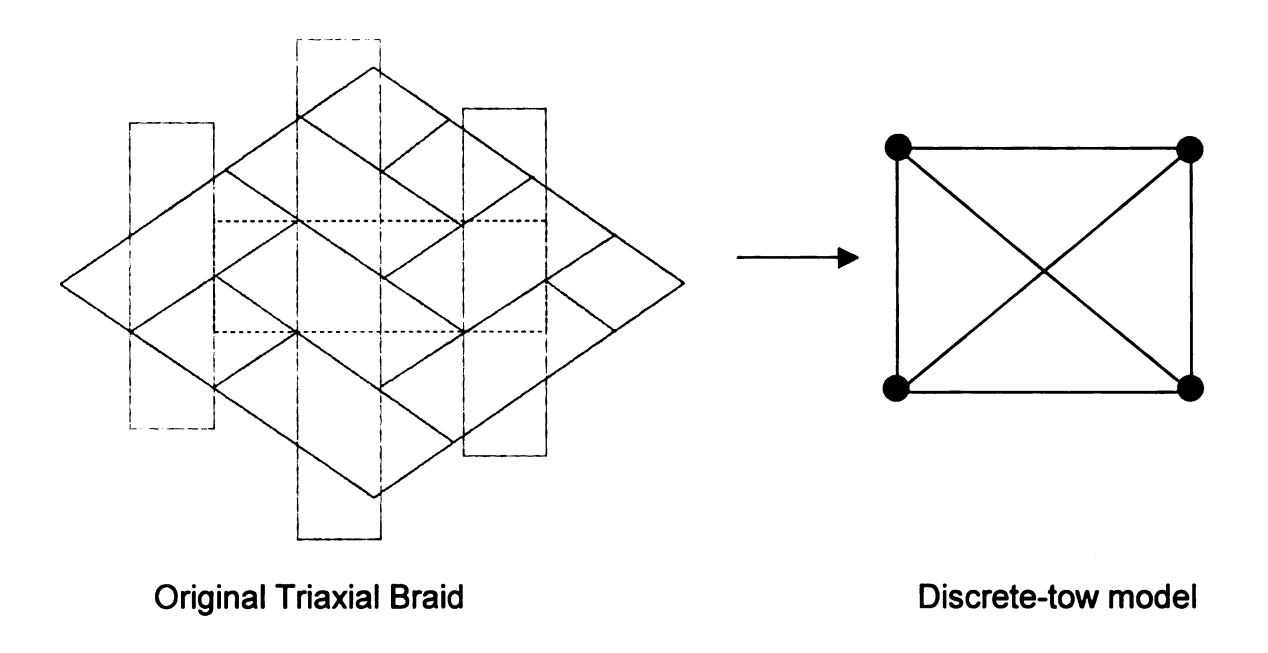


Figure 2.1 A summary of the modeling procedure from the isolation of a unit cell of a triaxially-braided composite material to the final discrete-tow model.

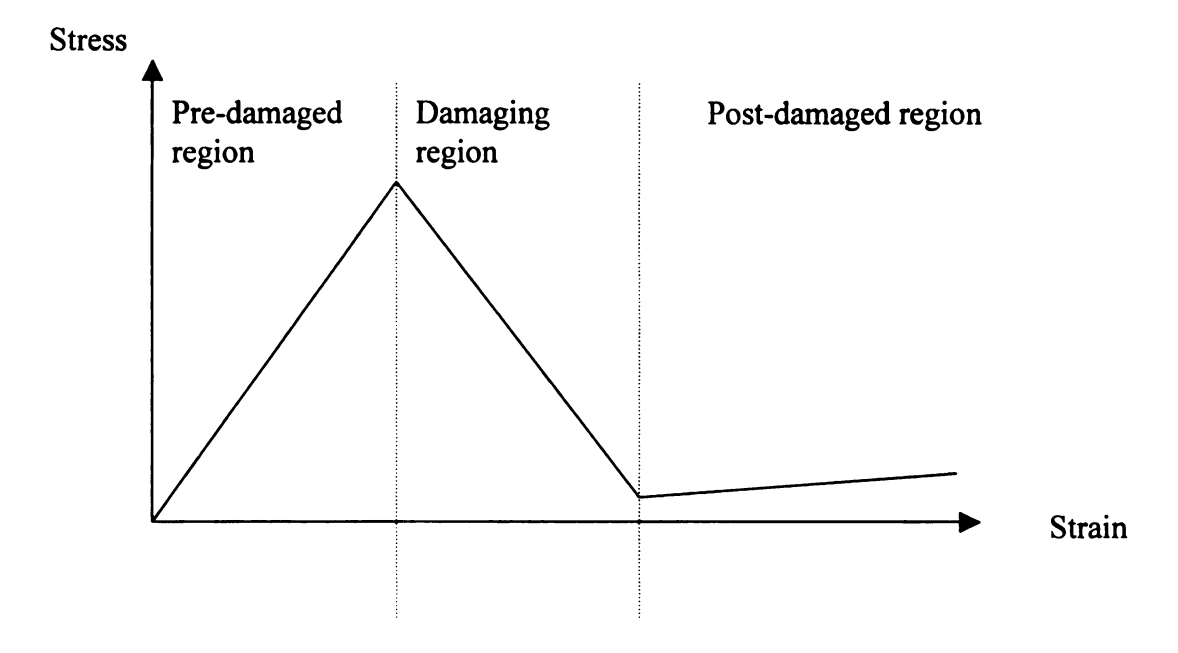


Figure 2.2 Damaging scheme of individual shell and beam elements in the discrete-tow model.

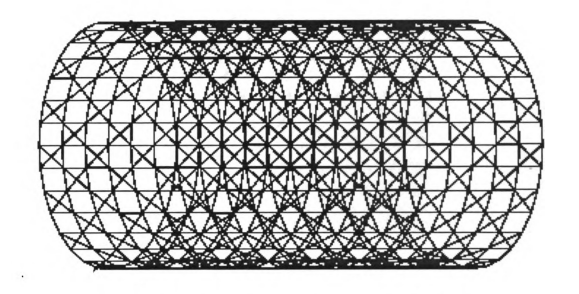


Figure 2.3 Crush tube model by the checkerboard model.

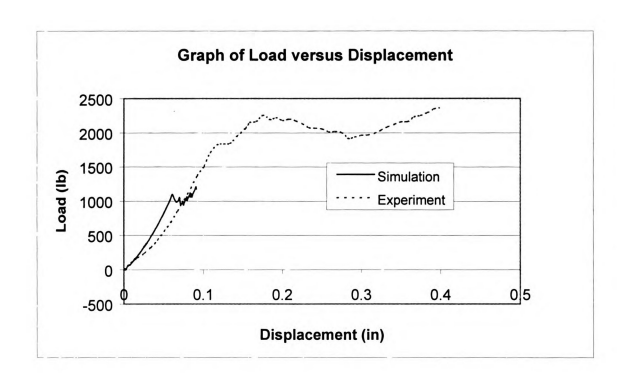
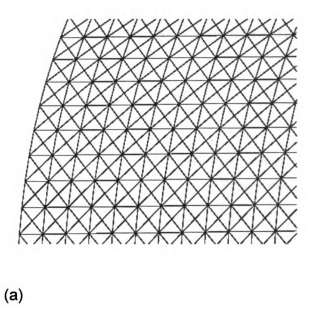
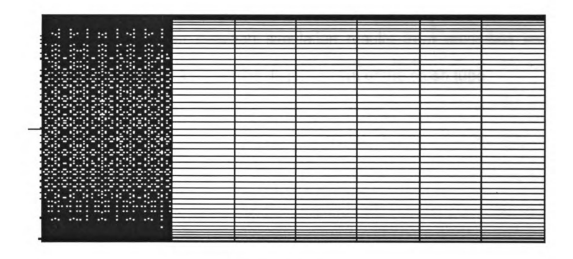


Figure 2.4 Comparison between simulation results from checkerboard model to experimental results of load versus displacement of the crush tube.





(b)

Figure 2.5 Crush tube modeled by the cross-box model. (a) A magnified view of the cross-box regions. (b) The whole crush tube, with cross-box region on the left.

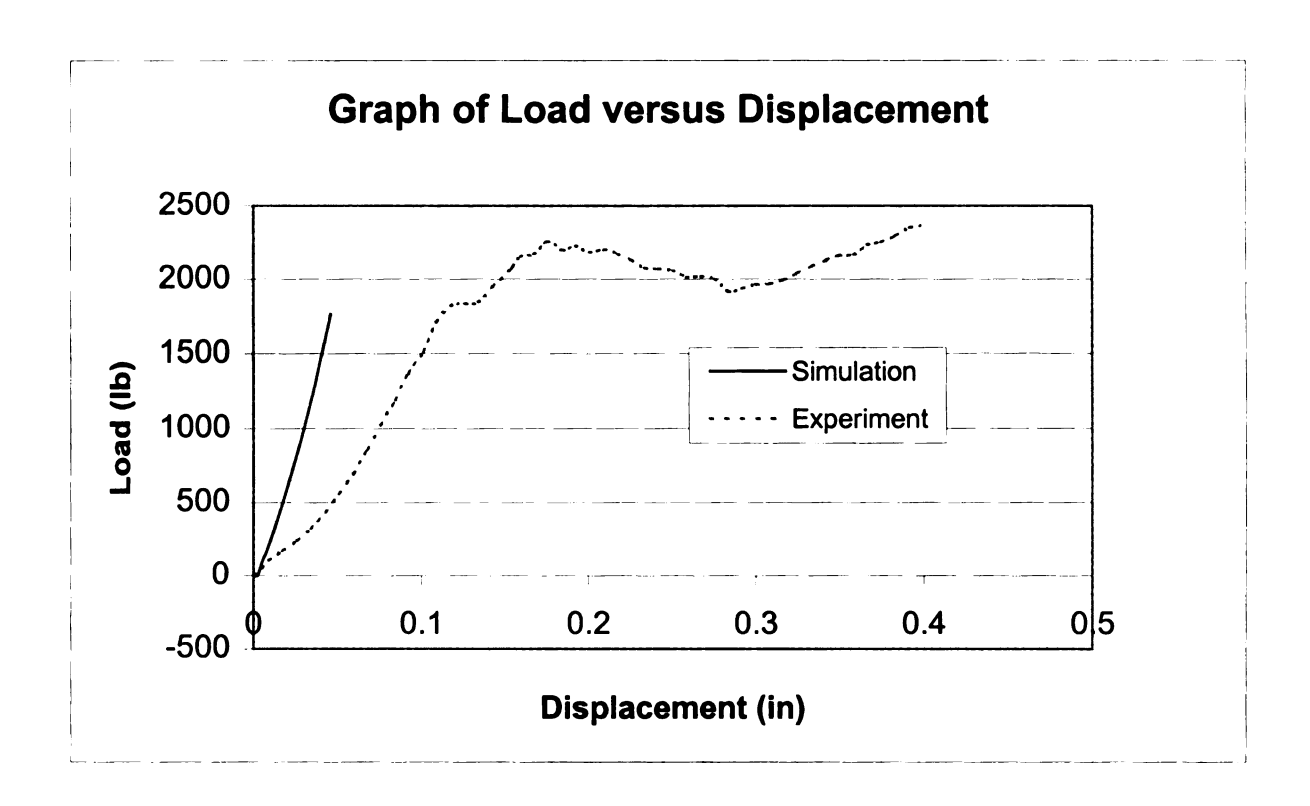


Figure 2.6 Comparison between simulation results from cross-box model to experimental results of load versus displacement of the crush tube.

Chapter 3

The Embedded-Tow Model

3.1 INTRODUCTION

Chapter 2 presented two modeling approaches, namely the checkerboard model and the cross-box model. These two models suffered from inaccurate predictions and divergence during the simulation analysis.

In this chapter, our final model—the embedded-tow model, will be introduced. This model is also inspired from the simplified discrete-tow model [29], and from the experience obtained after working on the two previous models. The embedded-tow model, as its name implies, implicitly represents the axial and braider tows in the shell elements. In other words, all three components in a unit cell—axial and braider tows, and matrix—are embedded in a shell element. Obviously, this model forfeits the benefits of explicitly modeling tow-scissoring and tow-sliding, since tows are not modeled discretely in the model. However, this model will be more computationally efficient, and will retain the capability to capture the failure of each tow discretely, providing that certain simplifying assumptions are reasonable from the engineering standpoint.

3.2 DESCRIPTION OF THE EMBEDDED-TOW MODEL

A quick review of the simplified discrete-tow model [29] will provide a better understanding of the current model. Details on computing the material stiffness matrix of the simplified discrete-tow model are also given in [29].

As shown in the discrete-tow model and again in Figure 3.1, one half of the repeating volume element of the triaxially-braided textile composite is sufficient for modeling the macro-mechanical properties of the overall textile composite. This repeating volume element can be further divided into two regions. One region contains the axial tow, as in the left region in Figure 3.1(b), and the other region does not. The stiffness matrix of each region is first computed using the classical laminate theory. The stiffness matrix of the overall composite is then computed by iso-stress and iso-strain assumptions.

The current approach adopts the same idea with respect to the computation of the material stiffness matrix. The overall composite macro-mechanical properties are assumed in each unit cell in our embedded-tow model. The embedded-tow model also retains the discrete-tow model capability of modeling tow undulation.

Due to the problem of divergence in the previous analyses using ABAQUS/IMPLICIT, the current model will be implemented within ABAQUS/EXPLICIT. Even though ABAQUS/EXPLICIT is more commonly used

for dynamic analysis, with proper mass scaling and loading rate, quasi-static analysis can be performed with sufficient accuracy.

3.2.1 ESTIMATING STRAINS OF INDIVIDUAL COMPONENTS

In this model, the individual strains of the axial tows, the braider tows and the matrix are first predicted with certain simplifying assumptions. These simplifying assumptions originate from the work of Mauget et al [41]. Since each unit cell will be represented by a reduced-integration shell element with a single in-plane integration point (five section points through thickness), and by intuition the deformation of the shell elements will be similar to that of an elementary box as described in [40], the work of these researchers can be adopted in the current model. Consequently, the idea presented by Mauget et al. can be used to describe shell deformation behavior of the current study with reasonable accuracy only before failure. Shell deformation after failure is hard to predict, but is not of major concern in our present study.

Figure 3.2 illustrates the presumed deformation of a shell element, or a unit cell, before failure. Using the infinitesimal strain assumption, the strain of both the axial tows in a unit cell can therefore be estimated to be equal to the shell strain along the loading direction, or its axial strain. The strain of the braider tows can be computed from the shell axial strain, transverse strain and shear strain using the strain transformation as stated in equation (3.1).

$$\varepsilon_{45} = \frac{\varepsilon_0 + \varepsilon_{90}}{2} + \frac{\varepsilon_0 - \varepsilon_{90}}{2} \cos(\pi) + \frac{\gamma}{2} \sin(\pi) \tag{3.1}$$

 ϵ_{45} is the strain of the braider tow, ϵ_0 and ϵ_{90} are the strains of the shell element in the loading and transverse directions, and γ is the shear strain of the shell element. It is important to point out that owing to the abovementioned assumptions and the use of one-integration-point element, the two axial tows in the unit cell will fail simultaneously. Similarly, the two braider-tows in the unit cell will fail at the same time. This approach is not general, but it provides an efficient method for modeling the crush tube of interest here.

3.2.2 PROGRESSIVE FAILURE SCHEMES OF INDIVIDUAL COMPONENTS

The discrete-tow model adopts the progressive failure scheme shown in Figure 2.2 for its constituents—the tows and the matrix, both in tension and compression. The current model will also account for failure of each constituent, but this time employing a different failure scheme for tensile and compressive loadings.

In tensile loading, the same progressive failure scheme as proposed in the discrete-tow model is employed. However, in compressive loading, the progressive failure scheme consists of only two regions instead of three, namely the pre-damaged and post-damaged regions, as shown in Figure 3.3. This modification is needed because constituents failing under compression are still

able to carry load. Post-damage load will compact the materials, instead of pulling them apart as in tensile loading. The compacted material can transfer additional load.

3.2.2.1 PROGRESSIVE FAILURE ALGORITHM

Since the textile composite material of the crush tube is non-linear in behavior, a FORTRAN algorithm has been written to simulate its behavior. This algorithm is incorporated into ABAQUS/EXPLICIT as a user subroutine called VUMAT. Both ABAQUS/IMPLICIT and ABAQUS/EXPLICIT provide its users the utility to include user materials, although the user-program interface of the software codes is different.

An incremental displacement approach is employed in the current quasistatic contact analysis. Description of the analysis is provided in section 3.2.3. As the initiator moves incrementally towards the crush tube, the resulting incremental crushing load is computed. The contact between the initiator and the crush tube produces incremental strains and stresses in the tows and matrix, which in the current analysis are embedded into the shell elements. These constituent materials fail progressively by their individual failure criteria, according to the aforementioned failure scheme. Similar to the analyses described in Chapter 2, the tows are assumed to obey a maximum strain failure criterion and the matrix a maximum stress failure criterion. When a material point fails, its stiffness is recomputed following the progressive failure scheme. The analysis then proceeds to redistribute the load around the failed site and continues with a new displacement increment. The algorithm is briefly summarized in Figure 3.4.

3.2.3 DESCRIPTION OF THE ANALYSIS

A quasi-static contact analysis is performed to simulate the crush tube behavior under compression. Figure 3.5 (a) shows a crush tube subjected to compressive force through a moving platen. Figure 3.5 (b) shows the equivalent model employed in the current analysis. An initiator was used in the experiment and in the simulation to prevent the onset of buckling and the occurrence of sudden peak force. It is noted that in the simulation, the initiator is moved incrementally towards the crush tube and the tube is fixed at its location. In the experiment, however, the initiator remains fixed while the crush tube was moved towards the initiator.

The initiator in the current simulation is modeled using an analytical rigid surface. This rigid surface is associated to a single node in all its movements and resulting forces. This provides the convenience of outputting the resulting force and displacement of the crush tube through a single node.

The initiator was positioned to establish immediate contact with the crush tube at the beginning of the simulation. The curvature of the initiator is 5/16 inch.

Since immediate contact was assumed, the initiator diameter is the diameter of the tube less its thickness. The tube diameter is 2.47 inches and its thickness is 0.075 inch. The crush tube has a chamfer at the crush end. The crush tube is made of 0°/+45°/-45° triaxially-braided composite material with 80k Fortafil #556 axial fibers, 12k Grafil 34-700 braider fibers and Ashland Hetron 922 epoxy vinyl ester as its matrix. The experimental density of the material is 1.4204E-4 lbf*s²/in⁴.

The size of unit cells used for the mesh of the tube is 0.075X0.075X0.075 cubic inch. This unit cell size was adopted assuming that the length of the chamfer is the same as that of one unit cell.

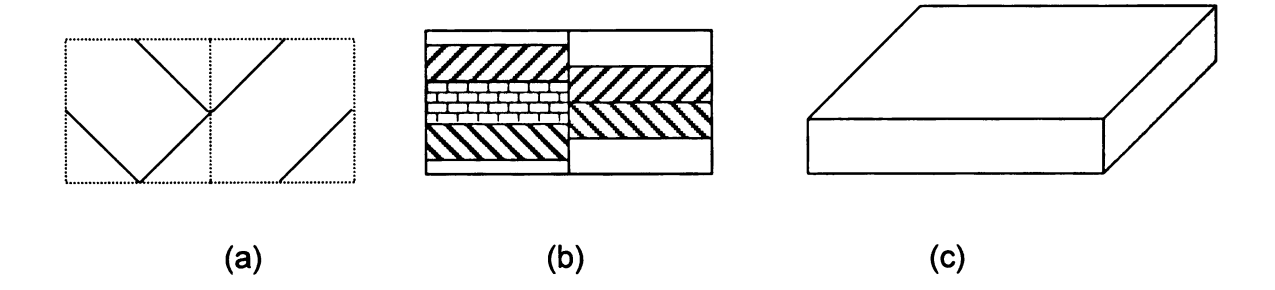


Figure 3.1 (a) Half of a repetitive volume element; (b) Axial tows, braider tows and resin represented as material stacks before the application of classical laminate theory; (c) The overall anisotropic material block, as in a unit cell.

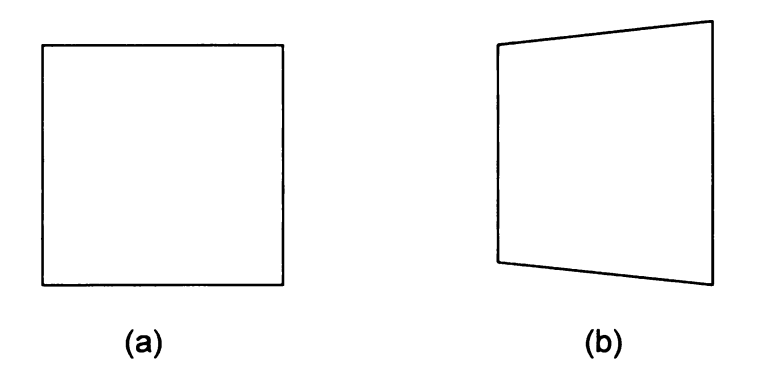


Figure 3.2 (a) Unit cell before deformation; (b) Unit cell after deformation.

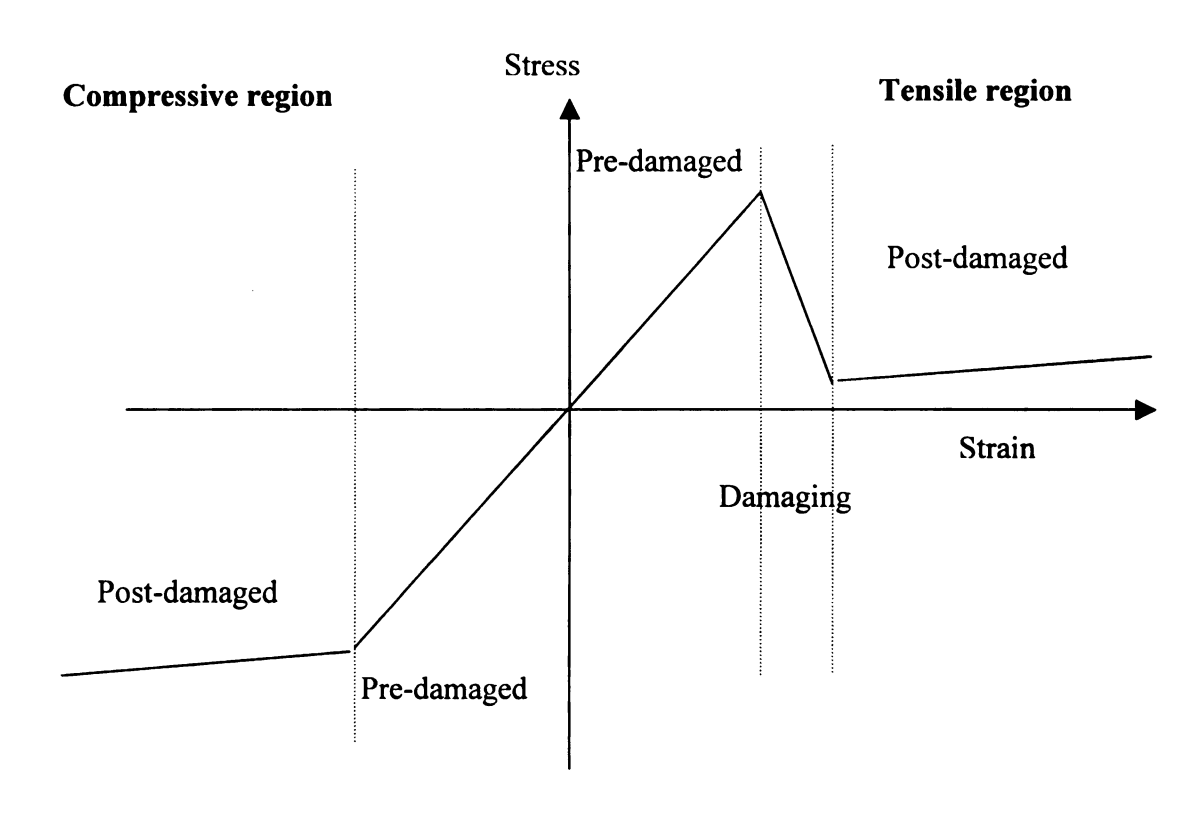


Figure 3.3 A stress-strain curve representing progressive failure scheme of each individual constituent in a unit cell.

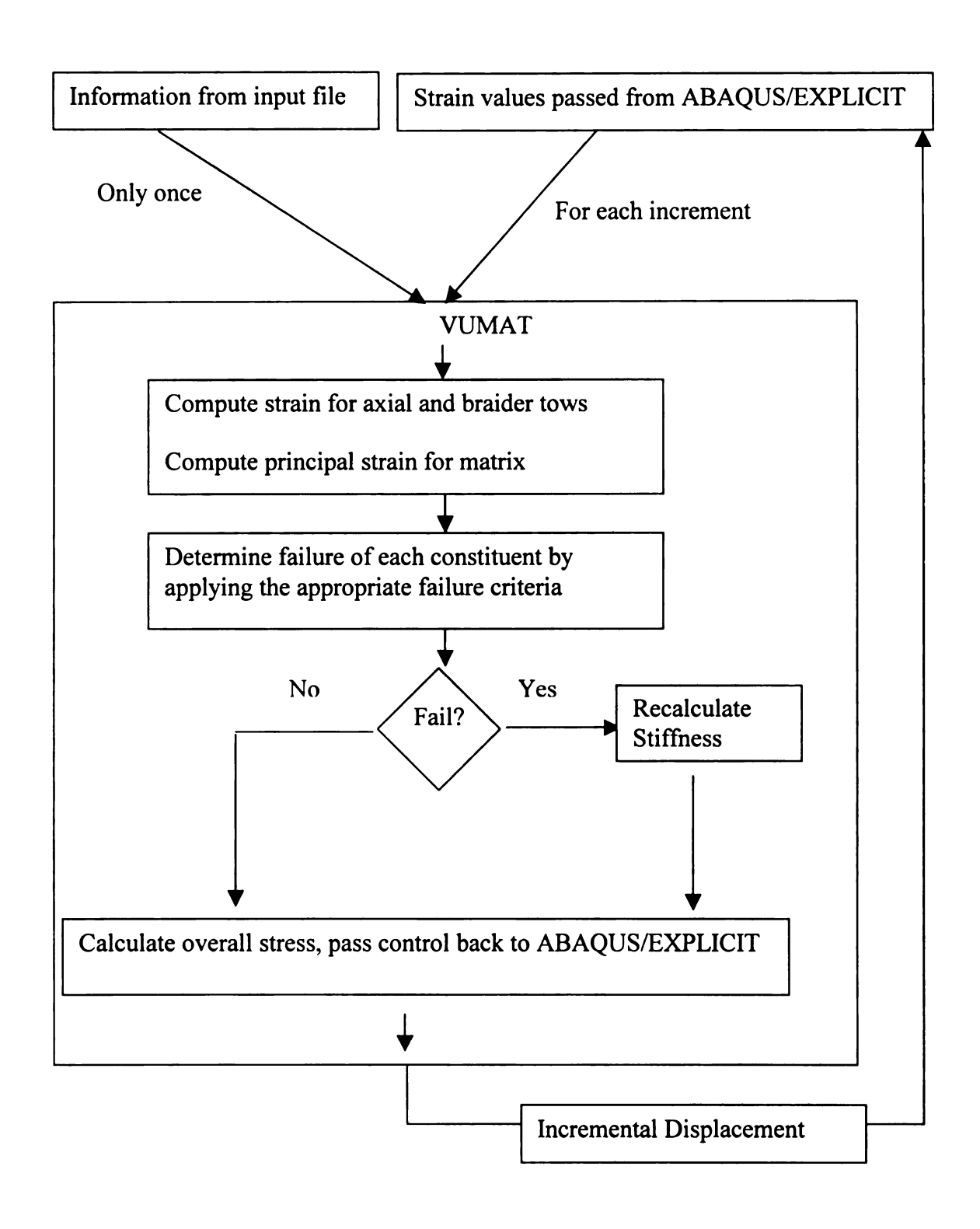
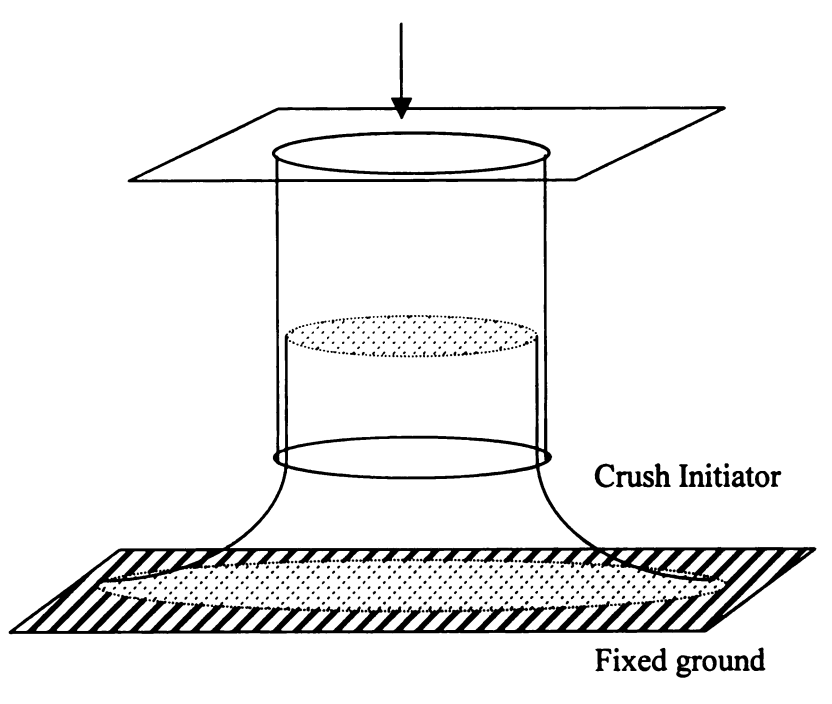


Figure 3.4 A summary of the progressive failure algorithm.

(a) Applied force applied to the platen in contact with tube



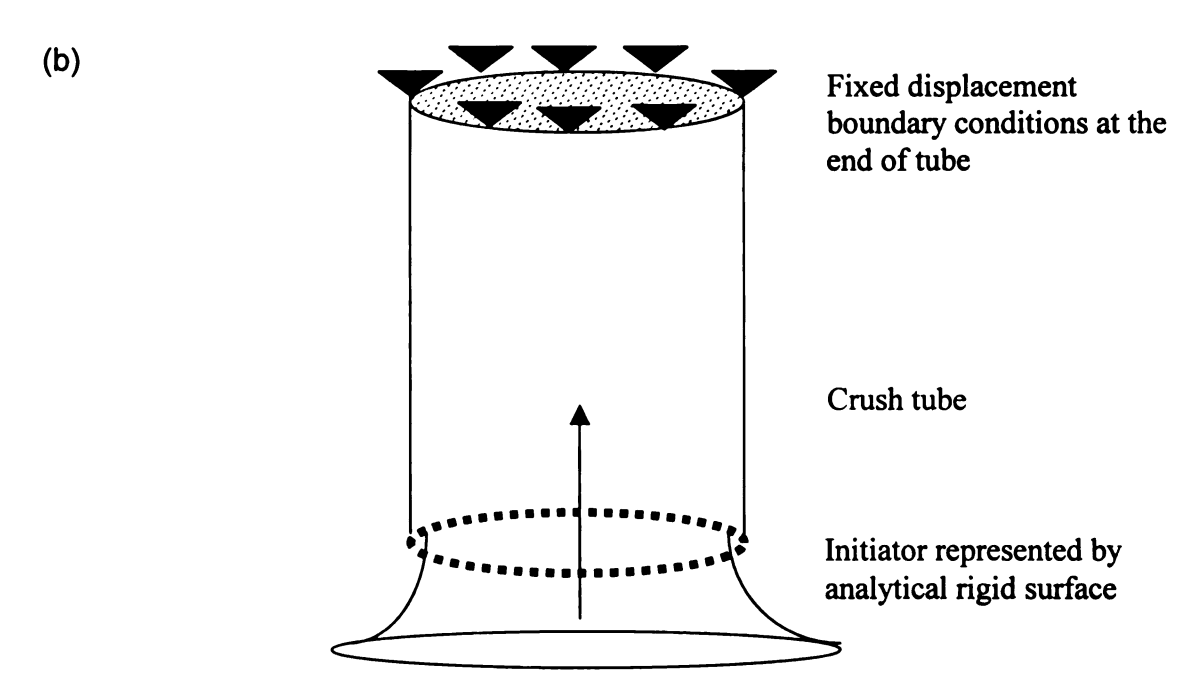


Figure 3.5 (a) Force applied at the platen, which moves towards the initiator, as in the experiment. (b) Initiator moves towards the tube in current simulation.

Chapter 4

Embedded-Tow Model Verification and Crush Tube Simulation Numerical Results

4.1 INTRODUCTION

Chapter 3 described the development of the embedded-tow model and how it could be used to model the crush tube behavior. This chapter attempts to verify the use of the embedded-tow model by demonstrating its accuracy in a simple bending situation whose analytical results can be obtained. The modeling of the progressive failure scheme is also verified by applying simple uniaxial tension and compression on a unit cell.

Since ABAQUS/EXPLICIT was used to simulate the force-displacement behavior of the tube, whose behavior is quasi-static, the effects of loading rate and mass scaling were also studied by performing simple bending analyses. Finally, an appropriate loading rate and mass scaling were chosen to simulate the crush tube under uniaxial compression. The appropriateness of the chosen loading rate and mass scaling can best be assured by detecting the simulated tube behavior for dynamic effects. The result was then plotted against the experimental crush tube behavior.

4.2 MATERIAL PROPERTIES

The elastic macro-mechanical properties of a unit cell used in all the analyses in this chapter are the same as that computed for the of 0°/+45°/-45° triaxially-braided composite material of the crush tube, and are summarized in Table 4.1. These values were computed from the mechanical properties of the composite constituents as listed Table 4.2 using the micro-mechanics approach adopted by Carrier and Averill [29]. The transverse shear stiffness of the composite is assumed to be the same as its in-plane shear stiffness in the absence of measured and simulated data, though this may give rise to stiffer analytical results as compared to the theoretical ones.

It is important to note that these values are only the elastic properties of the composite. Upon damage, the composite will behave non-linearly according to the progressive failure scheme outlined in Chapter 3 and thus the tabulated stiffness values will no longer apply. The constituent tows are assumed to be transversely isotropic and the matrix to be isotropic. The failure stress of matrix and the failure strain of axial and braider strains are also listed in Table 4.2.

4.3 VERIFICATION OF THE EMBEDDED-TOW MODEL

Three simple loading situations have been designed to verify the embedded-tow model behavior in the elastic and the past failure range. To simulate the model behavior in the elastic range, a simple bending analysis was performed on a strip of shell elements. To study the inelastic behavior of the model, simple uniaxial tension and compression tests were conducted on a unit cell, or a shell element. The simulated results were then compared with the theoretical results to verify the model usefulness.

4.3.1 SIMPLE BENDING ON A STRIP

A row of 54 0.75 in X 0.75 in X 0.75 in shell elements were connected end-to-end to form a strip whose length is 4.05 inches, that is about the same as the length of the 4-inch tube. A concentrated load was applied at one end, with the other end fixed as shown in Figure 4.1. The load was applied in a ramp fashion. The loading rate employed was small enough to ensure minimal dynamic effects. Any dynamic effects induced, as can only be observed from the strip response after the simulation, will disqualify the analysis from being quasistatic. The axial stress of the element at the fixed end and the out-of-plane displacement of the loaded end were obtained and compared to the theoretical results available from the theory of elementary strength of materials. According to this theory.

$$\delta = \frac{PL^3}{3E_x I_{vv}} \tag{4.1}$$

$$\sigma_x = \frac{PL(t/2)}{I_{yy}} \tag{4.2}$$

where δ is the out-of-plane deflection, P is the force applied at one end, E_x is the Young's Modulus along the strip direction, I_{yy} is the second moment of area along the y direction as consistent with Figure 4.1, and t is the thickness of the strip. At a loading rate of 0.2 lb/s, the simulated and theoretical displacements are compared in Figure 4.2. Note that the two lines lie closely on top of one another, indicating the accuracy of the embedded-tow model. Similarly, the simulated bending axial stresses of the element at the fixed end also agree closely with the theoretical values, as shown in Figure 4.3.

4.3.2 SIMPLE TENSION AND COMPRESSION ON A UNIT CELL

A 0.075 in X 0.075 in X 0.075 in shell element was subjected to uniaxial tensile and compressive stresses as depicted in Figure 4.4. The unit cell was stretched or compressed till damaged. Its tensile and compressive non-linear behavior is plotted in Figure 4.5 and Figure 4.6, respectively. The damage of the constituents was obvious as seen in the drop of the stress carried by the element. In tension, the axial tows in the unit cell were first observed to have

been damaged, followed by the matrix and finally the braider tows. In compression, however, the axial tow damage was followed by almost simultaneous damage of braider tows and matrix. The damaging behavior of the two different progressive failure schemes adopted for tensile and compressive loadings was clearly shown in these two figures. Note that the stress carried by the element after compressive failure remains unchanged, while tensile failure will render the element to carry less stress.

4.4. EFFECTS OF LOADING RATE AND MASS-SCALING

An inappropriate loading rate may induce dynamic effects in the computer analysis. Since the current analysis is quasi-static in nature, dynamic response is not desirable. This dynamic response can only be minimized by employing a low loading rate in the simulation. However, a low loading rate usually means greater computational efforts, and may render the analysis impractical if its computation time is too long. There is a trade-off between accuracy and computational effort. To accurately simulate the crush tube behavior in a significantly less amount of time, the use of mass scaling seems inevitable.

Mass scaling has the effect of speeding up the analysis. This is done by artificially increasing the material density by a factor of f so that the number of increments, n, of the analysis may be reduced to n/f. Basically, mass scaling reduces the ratio of the event time to the time for wave propagation across an element while leaving the event time fixed, which allows rate-dependent behavior

to be included in the analysis. Mass scaling has exactly the same effect on inertia forces as speeding up the time of analysis [42]. If abused, however, it induces errors in the simulation results. Therefore effects of loading rate and mass scaling first need to be studied. This investigation has been done by performing the strip bending simulation as described in Section 4.3.1.

First, the effects of different loading rates were examined. Using three different loading rates of 0.2 lb/s, 1.0 lb/s and 30.0 lb/s, the out-of-plane displacements of the strip subjected to bending were plotted against the theoretical values in Figure 4.7. It is evident from this figure that the displacement for the highest loading case deviates very much from those of the other two cases with lower loading rates, whose results match closely with the theoretical predictions. Therefore, it is more accurate to use a low loading rate.

A high loading rate has been shown to yield erroneous results. On the other hand, mass scaling may be shown to produce similar undesirable dynamic response if abused. Using different mass scale factors, namely a multiplication factor of 100 and 1000 times this original mass, the same simple bending simulations were repeated. Results are presented in Figure 4.8, where the displacements of the first two cases, one without mass scaling and the other with a factor of 100, were closer to the predicted theoretical displacement as compared to the one with the highest mass scaling.

Figure 4.8 seems to suggest the existence of a threshold value for mass scaling. For the current problem definition, a mass scaling of 100 times the original mass is adopted to speed up the simulation of the crush tube, since it has been shown to work well in the case of simple bending. The appropriateness of the loading rate, however, can only be decided upon the completion of the simulation, whose result should demonstrate sufficient indication on whether or not the dynamic effects of the simulated behavior is critical. Dynamically induced crushing behavior usually includes sudden and non-symmetrical failure of strips of elements. This failure mechanism corresponds to the tube axial splitting, which in a quasi-static experiment, is only likely to happen gradually and symmetrically around the circular tube. A loading rate of 0.025 in/s was employed in the present study.

4.5. CRUSH TUBE NUMERICAL SIMULATION RESULTS

4.5.1 CRUSH TUBE FORCE VERSUS DISPLACEMENT CURVE AND DAMAGE MECHANISM

Apart from loading rate and mass scaling, there are two other important parameters in the crush tube analysis, namely the friction between the tube material and the surface of the initiator, and the way the 45° chamfer of the tube is modeled. The effect of friction and chamfer modeling are discussed in more details in the following section, "Parametric Studies". The crushing force versus displacement curve for a tube with the chamfer modeled with three shell elements, Coulomb friction of 0.3 between the tube material and the surface of

initiator, and a loading rate of 0.025 in/s is shown in Figure 4.9. The experimental results used throughout this chapter were obtained from [40].

It is apparent that the simulated tube stiffness is higher than that of the experiment. Before any explanation is attempted, it is evident from the experimental curve that the stiffness of the real tube gradually increases initially, as opposed to the almost linear stiffness of our simulated tube before the peak load. This might be caused by the looseness of fit between the crush tube and the initiator in the experiment. This inevitable physical reality might have caused the increasing initial stiffness as shown in the experimental curve. The parametric studies on the effect of chamfer modeling and friction also reveal that these parameters do affect the initial stiffness, and the peak stress of the simulated response.

The analysis terminated prematurely because of bad element distortion. The analysis could be restarted after deleting highly distorted elements by identifying a state variable for each element in the model as deletion flag at the very first step of the simulation. However, this was not done in the current studies.

Figure 4.10 is a replica of Figure 4.9 except that important points of failure of constituent elements in the textile composite tube are marked on the curve

with the corresponding curve region zoomed. The damage mechanism associated with these points are summarized as follows:

A: Axial tows in the chamfer begin damaging in compression

B: Matrix in the chamfer begins damaging in tension

C: Matrix in the chamfer is completely damaged in tension

D: Matrix in the chamfer begins damaging in compression

E (Peak point): No axial or braider tensile failure

F: Braider tows in chamfer start damaging and failing in compression

G: Axial and braider tows in chamfer begins damaging in tension

H: No shell elements damaged in a strip. A strip refers to shell elements connected along the axial direction of the tube.

1: Strips of material start damaging, indicating dynamic response

The results show that the sharp drop between E and G is due to the tensile damage of both the axial and braider tows, which could be caused by high hoop stress at the crushing end.

4.5.2 PARAMETRIC STUDIES

4.5.2.1 EFFECTS OF CHAMFER MODELING

Since crush will initiate at the chamfer because of its weak pointed end and its relative thinness compared to the rest of the tube, the initial response of

the tube is dependent on how the chamfer in modeled. The current study has investigated the effects of modeling the chamfer with different number of shell elements lengthwise. Three different models were adopted. The first model has one shell element lengthwise for the chamfer, the second has 3 shell elements, and the third has 6 shell elements. The shell elements were not offset to the edge of the tube as in the real physical tube, rather they were centered along the mid-plane of the tube material, as shown in Figure 4.9. The results in Figure 4.10 show that the initial stiffness of the tube reduces as more elements are used to model the chamfer. This is intuitive as a more refined mesh in the chamfer allows the pointed end and its vicinity to be represented more accurately and thus, damage is allowed to occur at individually smaller elements. Also, it is noted that modeling chamfer with fewer elements lengthwise will increase the peak load for the same reason as mentioned.

4.5.2.2 EFFECTS OF FRICTION

The Coulomb friction has been used in the current analyses to model the friction between the tube material and the surface of the initiator. Two different friction values of 0.1 and 0.3 were used to investigate the difference in the crushing response. The results were shown on Figure 4.13. Again, the analysis with a Coulomb friction of 0.1 terminated because of highly distorted elements. However, Figure 4.13 clearly shows that a reduction in Coulomb friction results in a reduced initial tube stiffness and a reduced peak force. This is intuitive, since friction contributes to crush energy, and is suspected by Mamalis et al. [34] to

account for 40% to 50% of the total crush energy. The points marked on the curve correspond to material failure as listed below:

- A: Matrix in chamfer damaged in tension and compression

 Axial tows damaged in compression
- B: Braider tows start damaging in tension and failing in compression

 Matrix starts to fail in tension
- C: Axial tows partly damaged and partly failed in tension
- D: Strips of braider tows and matrix fail in tension, indicating dynamic response

Again, the sharp drop from A to C is most likely due to the tensile damage of the axial and braider tows by high hoop stress at the crushing end.

Table 4.1 Computed macro-mechanical properties of the $0^{\circ}/+45^{\circ}/-45^{\circ}$ triaxially-braided composite material of the 80k/12k crush tube.

Macro-mechanical Properties	Values
Young's Modulus in the loading direction, E _x	10.23 Msi
Young's Modulus in the transverse direction, E _y	1.672 Msi
In-plane Poisson's ratio, v_{xy}	0.573
In-plane Shear Modulus, Gxy	1.262 Msi

Table 4.2 Mechanical properties of the composite constituents.

Constituent	Macro-mechanical Properties	Values
Tows	Young's Modulus in the loading direction, E _x	19 Msi
	Young's Modulus in the transverse direction, E _y	1.2 Msi
	In-plane Poisson's ratio, v_{xy}	0.3
	In-plane Shear Modulus, Gxy	0.65 Msi
	Tensile Failure Strain	0.01
	Compressive Failure Strain	4.05267E-2
Matrix	Young's Modulus	0.46 Msi
	In-plane Poisson's ratio, v_{xy}	0.35
	In-plane Shear Modulus, G _{xy}	0.17037 Msi
	Tensile and Compressive Failure Stress	5.4E-3 Msi

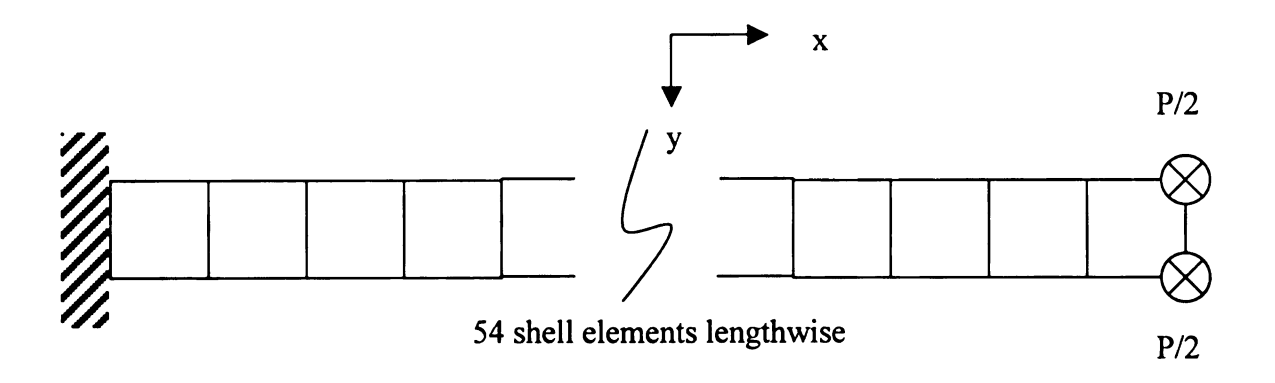


Figure 4.1 A simple bending analysis on a strip of shell elements. Two bending forces, each of P/2 in magnitude, were applied into the plane.

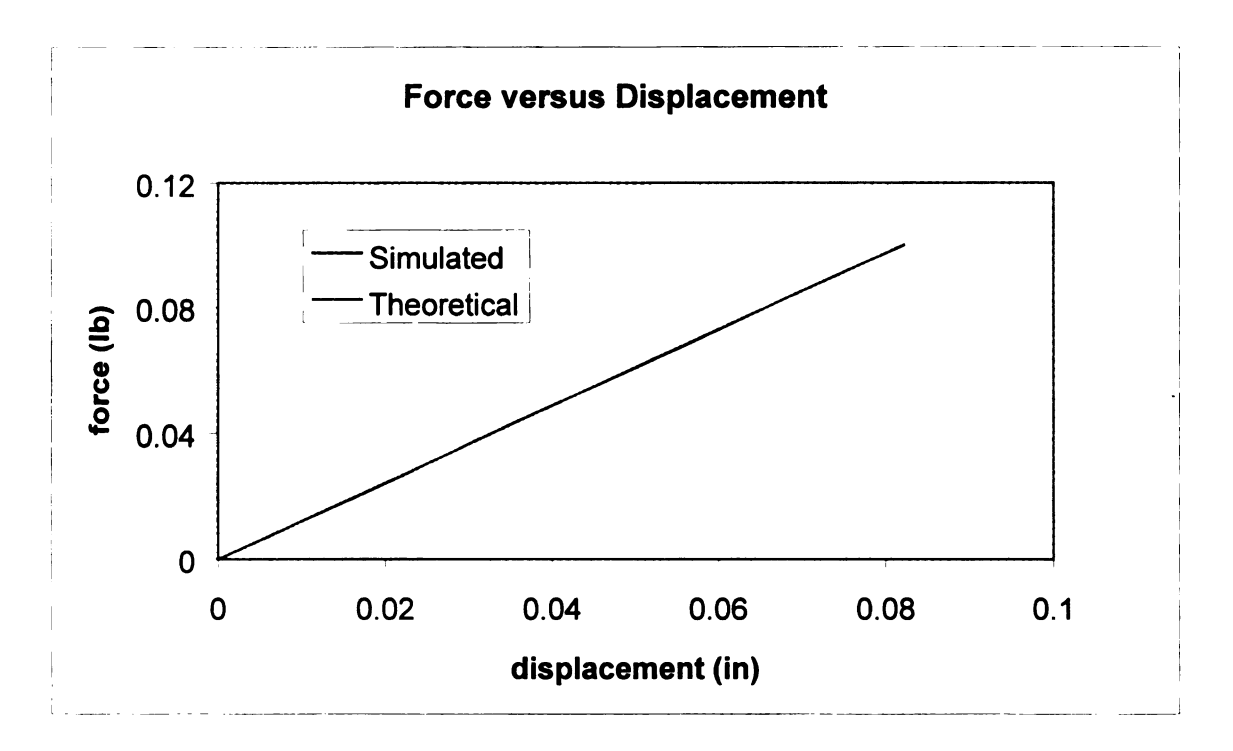


Figure 4.2 Comparison between the simulated and the theoretical out-of-plane displacements of the end of bending strip.

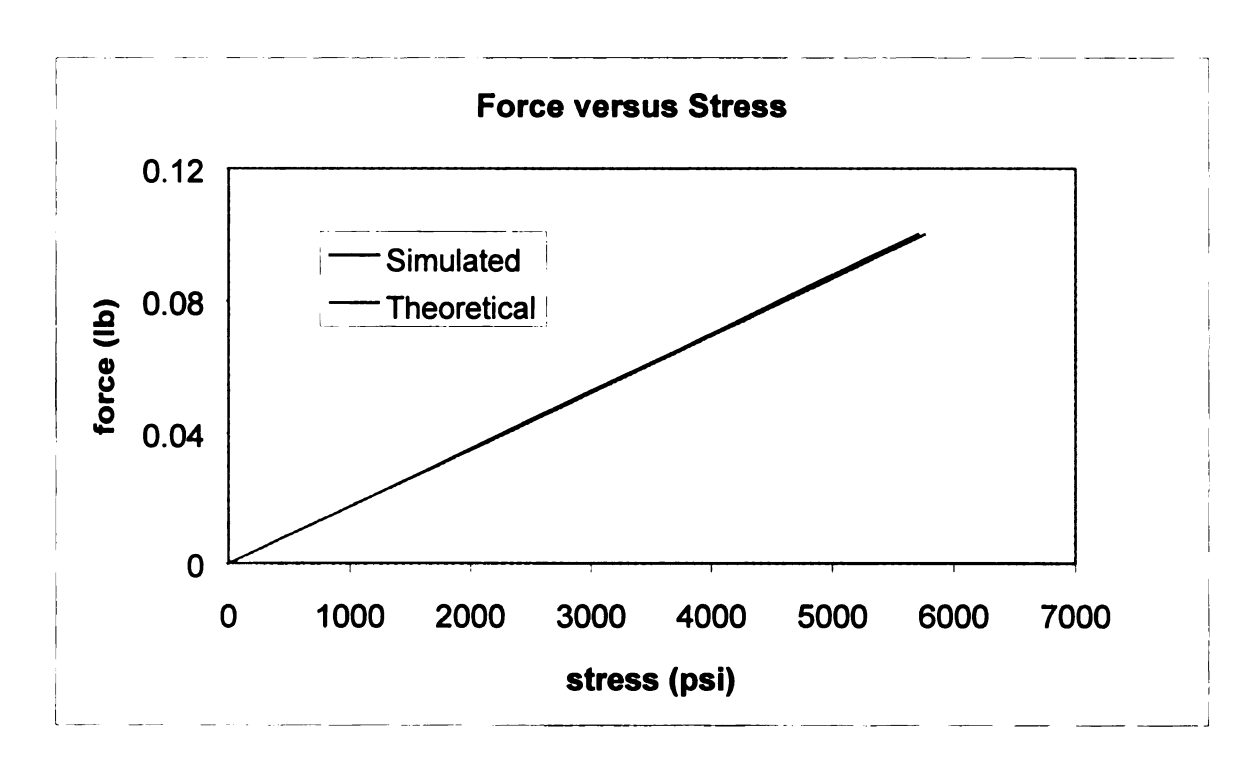


Figure 4.3 Comparison between the simulated and the theoretical bending stresses of the end of bending strip.

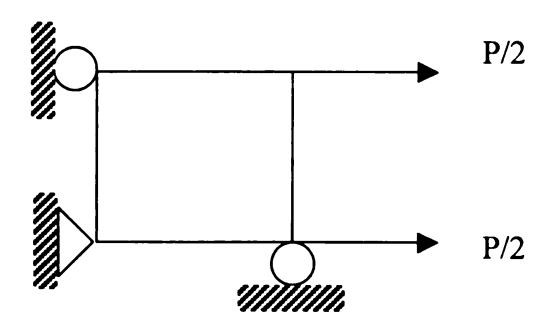


Figure 4.4 Uniaxial tensile and compressive test on a unit cell.

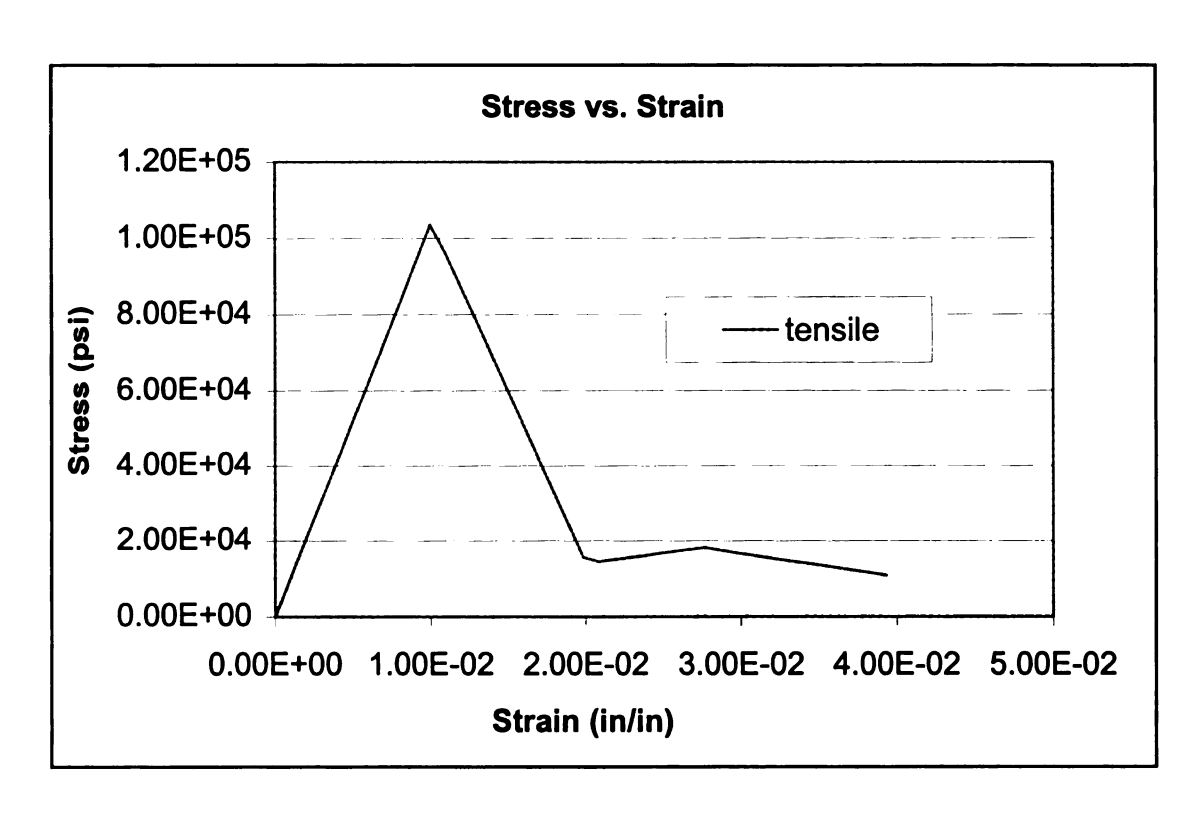


Figure 4.5 Stress-strain curve of a unit cell subjected to tensile force.

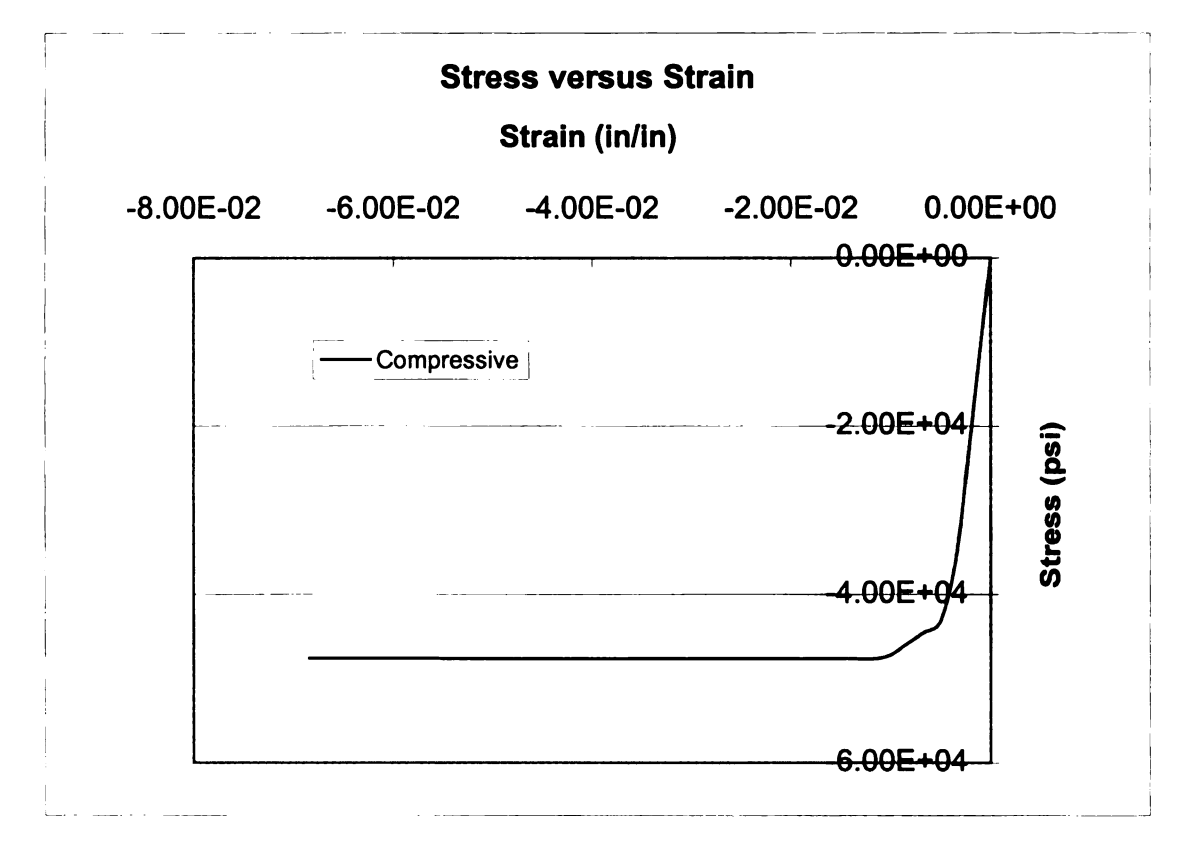


Figure 4.6 Stress-strain curve of a unit cell subjected to compressive force.

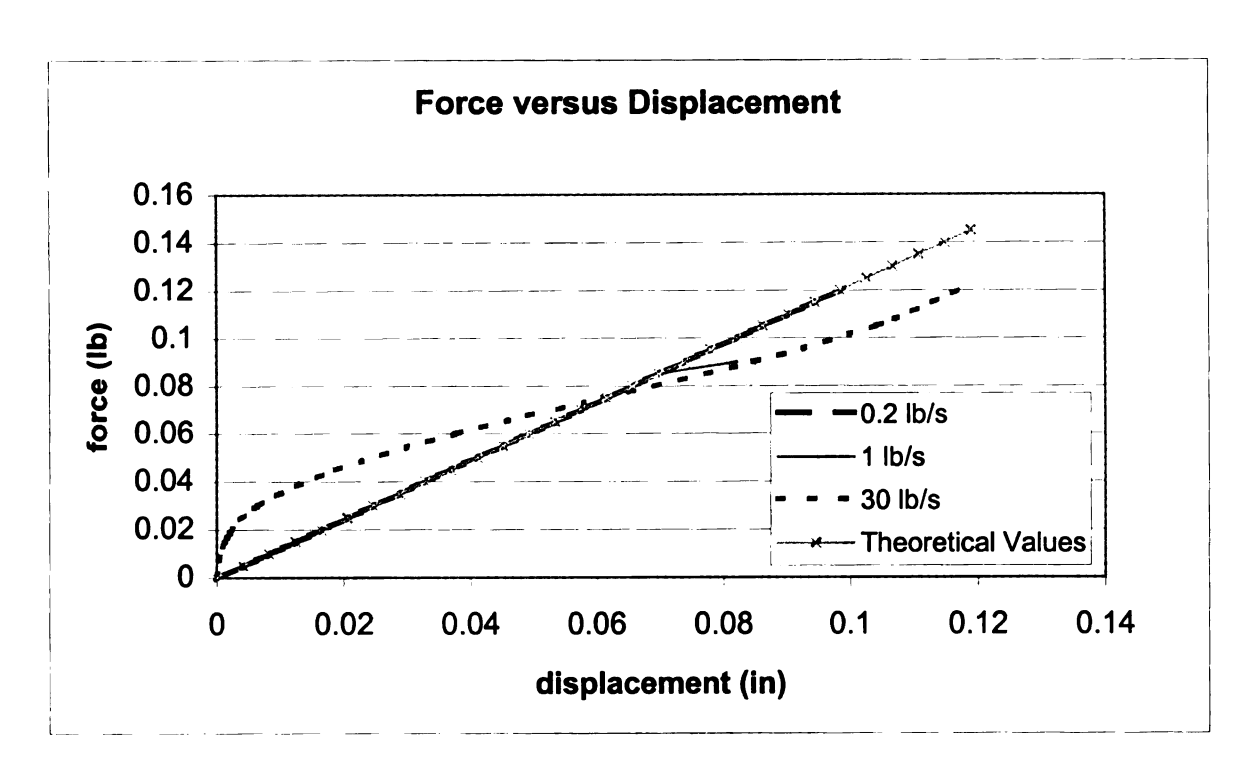


Figure 4.7 The effects of loading rate on the simulated strip out-of-plane displacement

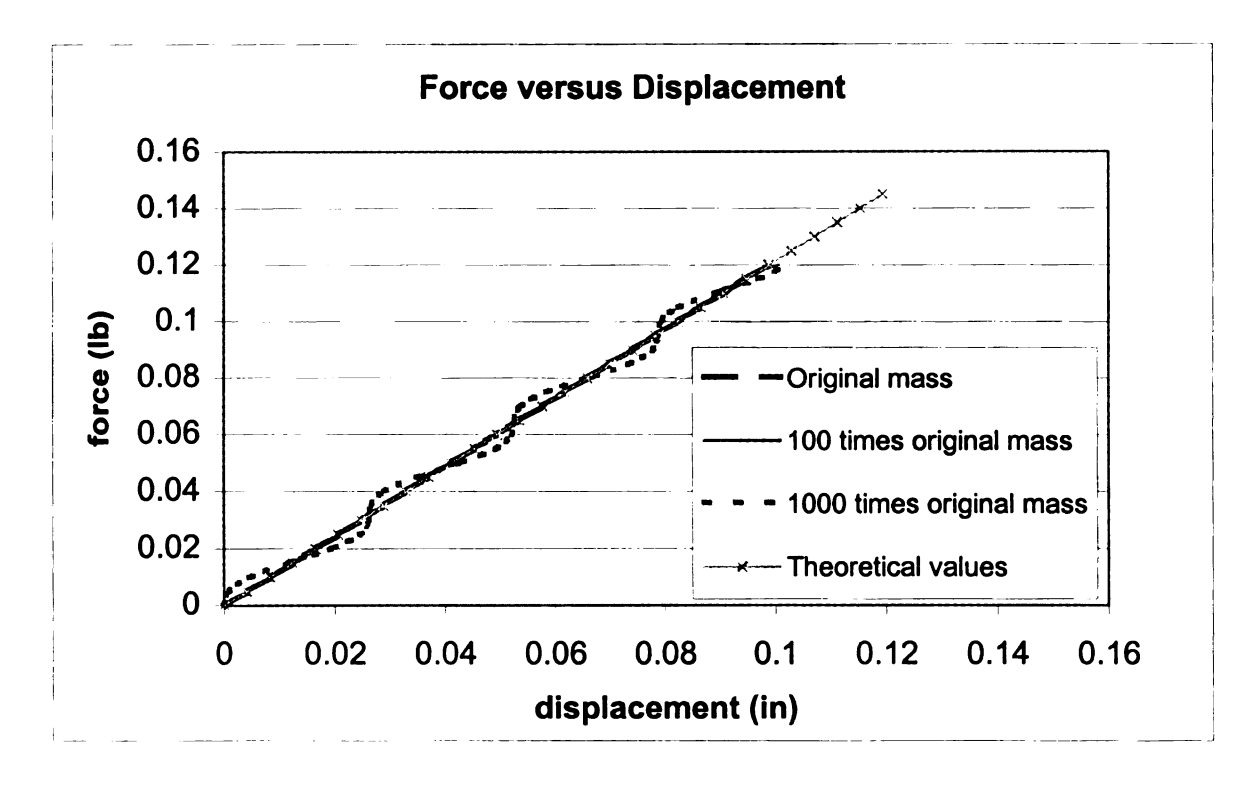


Figure 4.8 The effects of different mass scaling on the simulated strip out-ofplane displacement.

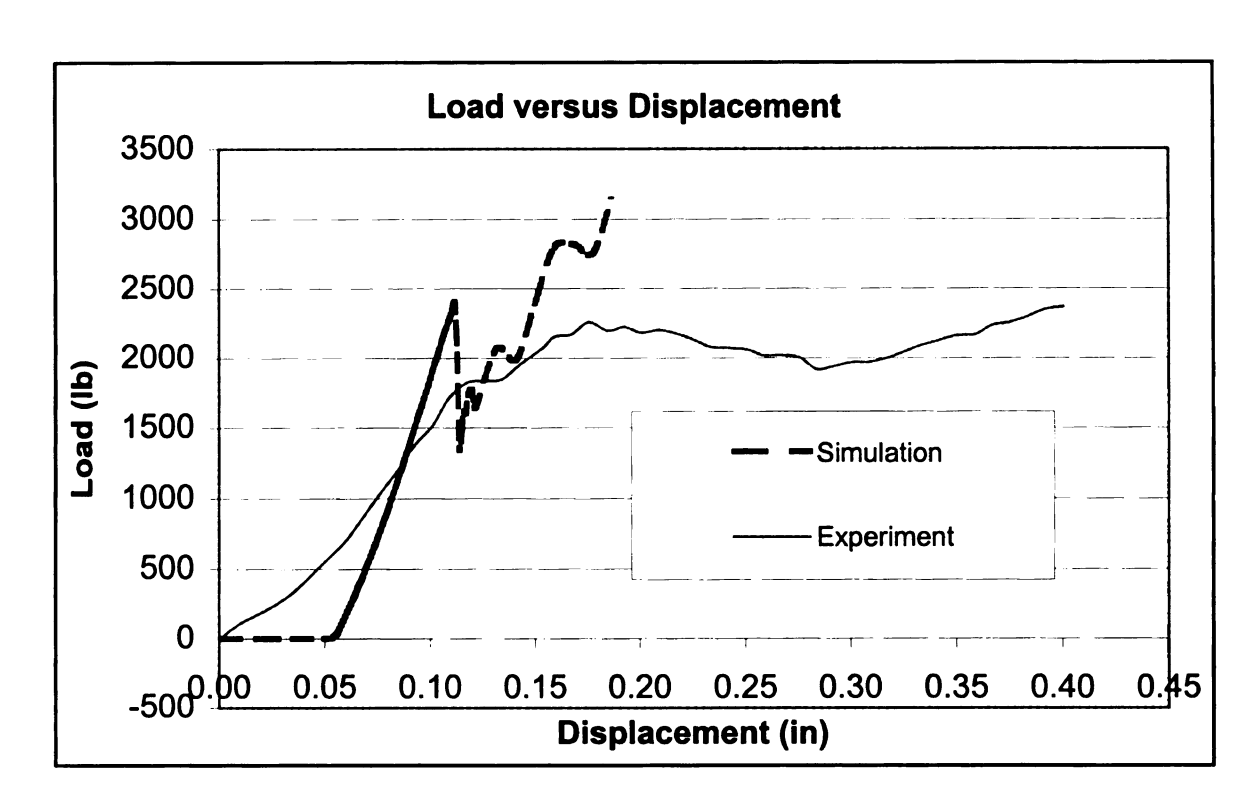


Figure 4.9 Simulated and experimental load versus displacement curves.

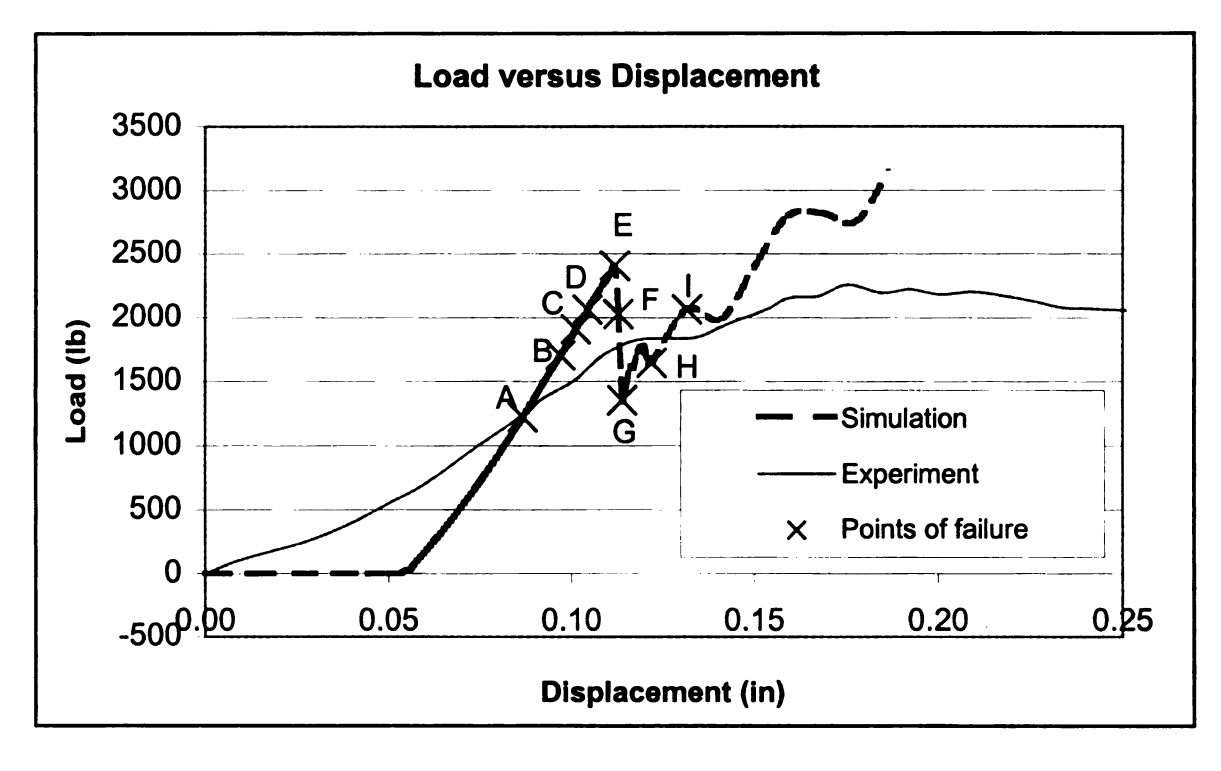


Figure 4.10 Simulated and experimental load versus displacement curves.

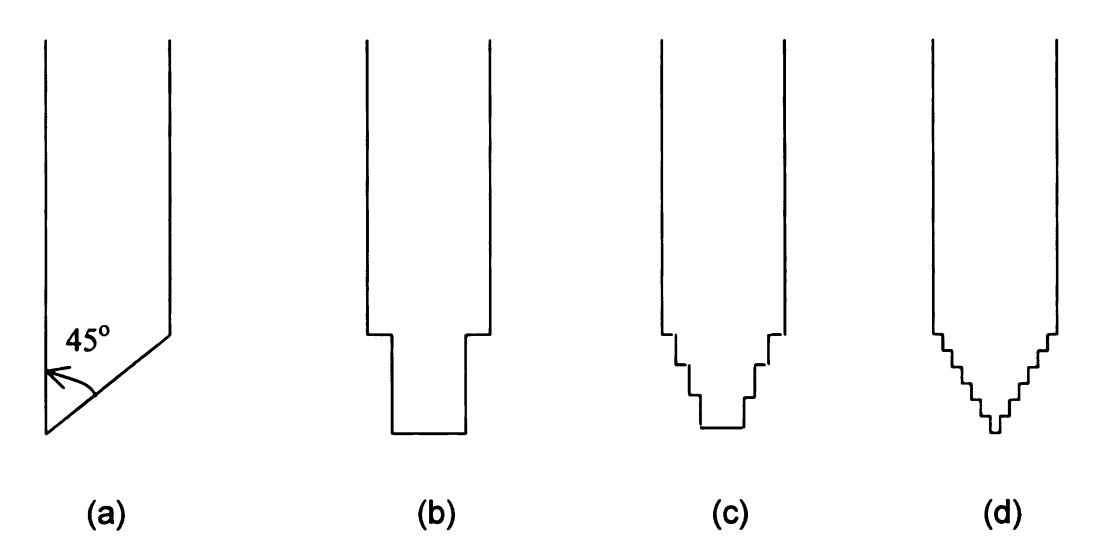


Figure 4.11 Modeling the chamfer. (a) The chamfer as in the tube specimen (b) Chamfer modeled with one shell element lengthwise (c) Chamfer modeled with three shell elements lengthwise (d) Chamfer modeled with six shell elements lengthwise.

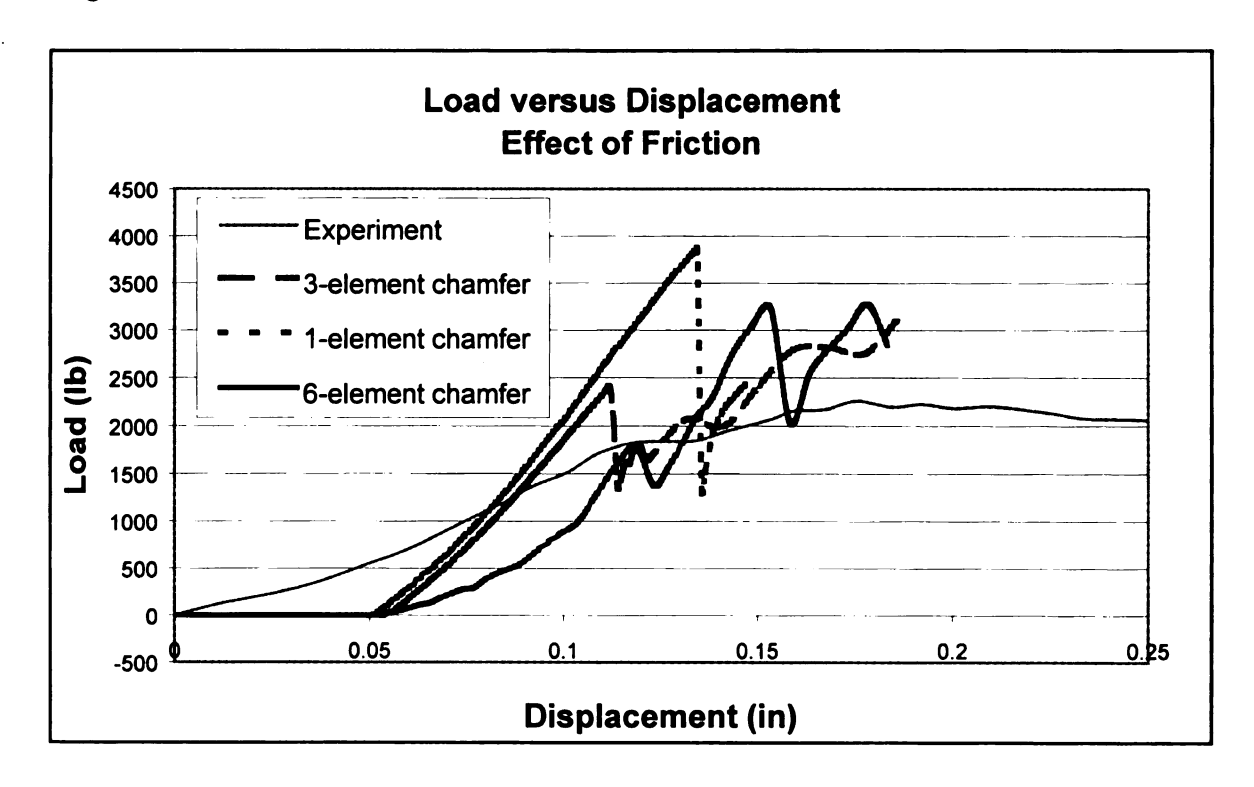


Figure 4.12 Effects of chamfer modeling on the load versus displacement curve.

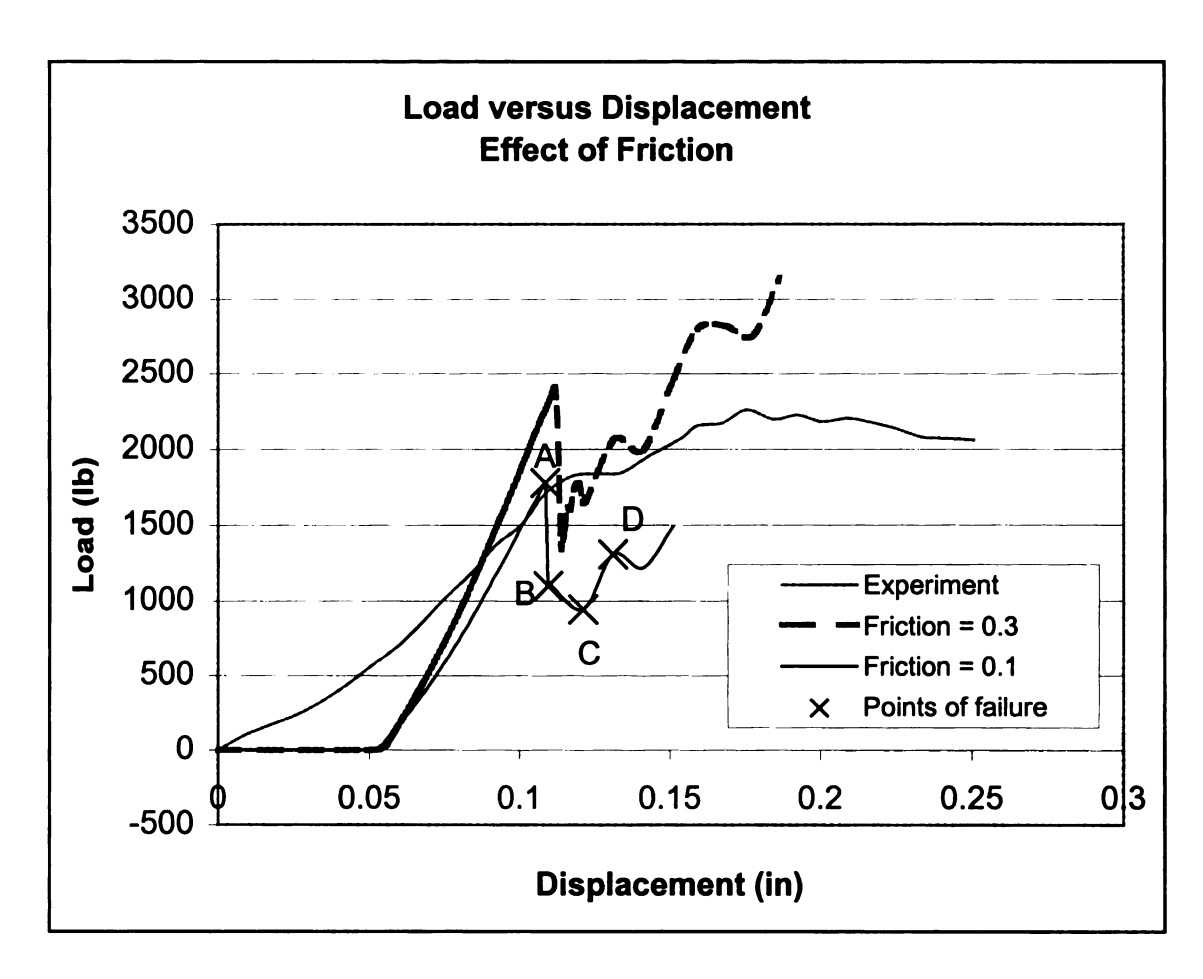


Figure 4.13 Effects of Coulomb friction on the load versus displacement curve.

Chapter 5

Conclusions

5.1 CONCLUSIONS

A method to efficiently model the crush simulation of triaxially-braided textile composite tubes was developed. The embedded-tow model has the ability to simulate the crush response of a circular tube, as demonstrated in the current study. The general trend of the numerical results agrees with that of the experiments. The use of this model may be extended for simulation of other general structures made of triaxially-braided textile composite. However, care has to be taken by considering the assumptions that go into the modeling of the crush tube. Though the crush tube model needs improvement in the modeling of chamfer to increase its accuracy in predicting the initial stiffness response, the embedded-tow model proves to be a promising tool for crushing analysis.

5.2 FUTURE WORK

To complete the analyses of the current studies, a state variable for each individual element has to be set apart as a deletion flag at the very beginning of the analyses. The embedded-tow model, though with much simplification, is still computationally consuming and may need further modification. This model has

also forfeited its parent model ability to represent the sliding of tows in the composite during crush by incorporating tows into shell elements. In addition, the current approach has neglected delamination in the composite material, which in reality occurs when the tube is crushed. Tow sliding and delamination are important parameters that affect the crush energy of the composite tube. Work has to be done to incorporate the effects of tow-sliding and delamination in this model.

Bibliography

1 Ishikawa, T. and Chou, T. W., "Elastic Behavior of Woven Hybrid Composites," *Journal of Composite Materials*, Vol. 16, 1982, p.2-19

2 Ishikawa, T. and Chou, T. W., "One-Dimensional Micromechanical Analysis of Woven Fabric Composites," *AIAA Journal*, Vol. 21, No. 12, 1983, pp. 1714-1721.

3 Ishikawa, T. and Chou, T. W., "Stiffness and Strength Behavior of Woven Fabric Composite," *Journal of Material Science*, Vol. 17, 1982, pp. 3211-3220.

4 Yang, J. M., Ma, C. L. and Chou, T. W., "Fiber Inclination Model of Three-Dimensional Textile Structural Composites," *Journal of Composite Material*, Vol. 20 (1986), pp. 472-484.

5 Whitcomb, J. D., "Three-dimensional Stress Analysis of Plain Weave Composites," *Composite Materials: Fatigue and Fracture*, Vol. 3, ASTM STP 1110, American Society for Testing and Materials, 1991, pp. 417-438.

6 Whitcomb, J., Woo, K., and Gundapaneni, S., "Macro Finite Element for Analysis of Textile Composites," *Journal of Composite Materials*, Vol. 28, No 7, 1994, pp. 607-618.

7 Woo, K., and Whitcomb, J., "Global/Local Finite Element Analysis for Textile Composites," *Journal of Composite Materials*, Vol. 28, No. 14, 1994, pp. 1305-1321.

8 Woo, Kyeongsik and Whitcomb. J, "Effects of Fiber Tow Misalignment on the Engineering Properties of Plain Weave Textile Composites," *Journal of Composite Structures*, Vol. 37, No 3/4, 1997, pp. 345-355.

9 Whitcomb, J. and Srirengan, K., "Simulation of Progressive Failure in Plain Weave Textile Composites," 1994 International Mechanical Engineering Congress and Exhibition, of the Winter Annual Meeting, AERO-2, 1994, pp. 1-13.

10 Whitcomb, J. and Srirengan, K., "Effect of Various Approximations on Predicted Progressive Failure in Plain Weave Composite," Journal of Composite Science, Vol. 34, 1996, pp. 13-20.

11 Ganesh, V. K. and Naik, N.K., "Failure behavior of plain weave fabric laminates under in-plane shear loading: effect of fabric geometry", *Composite Structures*, Vol. 30, 1995, p. 179-192.

- 12 Ganesh, V. K. and Naik, N. K., "Failure Behavior of Plain Weave Fabric Laminates under On-Axis Uniaxial Tensile Loading: I Laminate Geometry," *Journal of Composite Material*, Vol. 30, No.16, 1996, pp. 1748-1778.
- 13 Naik, N. K. and V. K. Ganesh, "Failure Behavior of Plain Weave Fabric Laminates Under On-Axis Uniaxial Tensile Loading: II Analytical Predictions," *Journal of Composite Materials*, Vol. 30, No. 16, 1996, pp. 1779-1822.
- 14 Ganesh, V. K., and Naik, N. K., "Failure Behavior of Plain Weave Fabric Laminates under On-Axis Uniaxial Tensile Loading: III Effect of Fabric Geometry," *Journal of Composite Materials*, Vol. 30, No. 16, 1996, pp. 1823-1834.
- 15 Naik, N. K., and Ganesh, V. K., "Failure Behavior of Plain Weave Fabric Laminates Under In-Plane Shear Loading," *Journal of Composites Technology & Research*, Vol. 16, No.1, 1994, pp. 3-20.
- 16 Naik, N.K. and Ganesh, V.K., "Prediction of On-axes Elastic Properties of Plain Weave Fabric Composites", *Composite Science and Technology*, Vol. 45, p. 135-152.
- 17 Naik, Rajiv A., Peter G. Ifju and John E. Masters, "Effect of Fiber Architecture Parameters on Deformation Fields and Elastic Moduli of 2-D Braided Composite", *Journal of Composite Materials*, Vol. 28, No 7, 1994, pp. 656-681.
- 18 Naik, Rajiv A. "Failure Analysis of Woven and Braided Fabric Reinforced Composites", *Journal of Composite Materials*, Vol. 29, No. 12, 1995, pp. 2334-2363.
- 19 Naik, Rajiv A., "Analysis of Woven and Braided Fabric-Reinforced Composites", *Composite Materials: Testing and Design,* Vol. 12, ASTM STP 1274, American Society for Testing and Materials, 1996, pp. 239-263.
- 20 Dasgupta, A., Bhandarkar, S., Pecht, M. and Barker, D., "Thermoelastic Properties of Woven-Fabric Composites Using Homogenization Techniques", Computer Aided Life Cycle Engineering Center, ME department, University of Maryland.
- 21 Takano, N., Uetsuji, Y., Kashiwagi, Y. and Zako, M., "Hierarchical Modeling of Textile Composite Materials and Structures by Homogenization Method," *Modelling and Simulation in Materials Science and Engineering*, 1999, pp. 207-231.

- 22 Sankar, Bhavani V. and Marrey, Ramesh V., "Analytical Method for Micromechanics of Textile Composites," *Journal of Composites Science and Technology*, Vol. 57, Elsevier Science Limited, 1997, pp. 703-713.
- 23 Pastore, Christopher M. and Yasser A. Gowayed, "A Self-Consistent Fabric Geometry Model: Modification and Application of a Fabric Geometry Model to Predict the Elastic Properties of Textile Composites", *Journal of Composites Technology & Research*, Vol. 16, No.1, January 1994, pp. 32-36.
- 24 Glaessgen, E. H., Pastore, C. M., Griffin, O. H. and Birger, A., "Geometrical and Finite Element Modeling of Textile Composite," *Composites Part B*, Vol. 27B, No. 1, 1996, pp.43-50.
- 25 Dadkhah, M. S., Flintoff, J. G., Kniveton, T. and Cox, B. N., "Simple Models for Triaxially Braided Composites," *Journal of Composites*, Vol. 26, Elsevier Science Limited, 1995, pp. 561-577.
- 26 West, A. C. and Adams, D. O., "Effect of Yarn Crimping on Compressive Strength Design Allowables of Braided Composites," *Textile Composites*, pp. 999-1006.
- 27 Masters, J. E., Foye, R. L., Pastore, C. M. and Gowayed, Y. A., "Mechanical Properties of Triaxially Braided Composites: Experimental and Analytical Results," *Journal of Composites Technology and Research*, Vol. 15, No. 2, Summer 1993, pp. 112-122.
- 28 Masters, E. John and Ifju, Peter G., "A Phenomenological Study of Triaxially Braided Textile Composites Loaded in Tension", *Composites Science and Technology*, Vol. 56, 1996, pp. 347-358.
- 29 Carrier, C.R and Averill, R., "A Simplified Discrete-tow Model for Modeling Stiffness and Failure within Woven Composites," *Journal of Composites Technology and Research*, Vol. 22, No. 4, October 2000, pp. 196-206.
- 30 Hamelin P. and Bigaud, D., "A Numerical Procedure for Elasticity and Failure Behavior Prediction of Textile-Reinforced Composite Materials," *Journal of Thermoplastic Composite Materials*, Vol. 12, May 1999, pp. 201-213.
- 31 Tan, S. C. and Nuismer, R. J., "A Theory for Progressive Matrix Cracking in Composite Laminates," *Journal of Composite Materials*, Vol. 23, Technomic Publishing Co. Inc., Oct 1989, pp. 1029-1047.
- 32 Blackketter, D.M., Walrath, D. E. and Hansen, A. C., "Modeling Damage in a Plain Weave Fabric-Reinfored Composite Material", *Journal of Composites Technology & Research*, JCTRER, Vol. 15, No. 2, Summer 1993, pp. 136-142.

- 33 Tan, P., L. Tong and Steven, G. P., "Modeling for Predicting the Mechanical Properties of Textile Composite-A Review", *Composites Part A*, Vol. 28A (1997), p. 903-922.
- 34 Mamalis, A. G., Manolakos, D. E., Demosthenous, G. A. and Ioannidis, M. B., *Crashworthiness of Composite Thin-Walled Structural Components*, Lancaster: Technomic Publishing Co. Inc., 1998.
- 35 Castején, L., Cuartero, J., Clemente, R. and Larrodé, E., "Energy Absorption Capability of Composite Materials Applied to Automotive Crash Absorbers Design", *SAE Journal*, 980964, Society of Automotive Engineers, Inc., 1998, pp. 716-724.
- 36 Hamada, H. and Nakatani, T., "Analysis of Crushing Mechanism on Composite Tube under Axial Load," *SAE Journal*, 970247, pp. 281-286.
- 37 Masters, J. E. and Minguet, P. J., "Effect of Preform Architecture on Modulus and Strength of Two-Dimensional, Triaxially Braided, Textile Composite Materials", Composite Materials: Testing and Design, Vol. 12, ASTM STP 1274, American Society for Testing and Materials, 1996, pp. 201-207.
- 38 Chiu, C.H., Tsai, K. H. and Huang, W. J., "Crush-failure Modes of 2D Triaxially Braided Hybrid Composite Tube," *Composite Science and Technology*, Vol. 59, 1999, pp. 1713-1723.
- 39 Hull, D., "A Unified Approach to Progressive Crushing of Fiber-Reinforced Composite Tubes," *Composites Science and Technology*, 1991, Vol. 40, pp. 377-421.
- 40 Beard, Shawn J., "Energy Absorption of Braided Composite Tubes," A Doctor of Philosophy Dissertation, Department of Aeronautics and Astronautics, Stanford University, April 2001, pp 1-140.
- 41 Mauget, B. R., Minnetyan, L. and Chamis, C. C., "Large Deformation Nonlinear Response of Soft Composite Structures via Laminate Analogy," *Proceedings of the 8th Japan-U.S. Conference On Composite Materials*, September 24-25, 1998, pp.147-156.
- 42 "Explicit Dynamic Analysis," *ABAQUS/Explicit User's Manual Version 5.6*, Vol. I, 1996, pp.6.2.1-8.

